



HAL
open science

An agent-based model of vibration-induced intimal hyperplasia

Maha Reda, Christophe Noël, Nicla Settembre, Jérôme Chambert, Arnaud Lejeune, Gwenaël Rolin, Emmanuelle Jacquet

► **To cite this version:**

Maha Reda, Christophe Noël, Nicla Settembre, Jérôme Chambert, Arnaud Lejeune, et al.. An agent-based model of vibration-induced intimal hyperplasia. *Biomechanics and Modeling in Mechanobiology*, 2022, 21 (5), pp.1457 - 1481. 10.1007/s10237-022-01601-5 . hal-04153796

HAL Id: hal-04153796

<https://hal.science/hal-04153796>

Submitted on 6 Jul 2023

HAL is a multi-disciplinary open access archive for the deposit and dissemination of scientific research documents, whether they are published or not. The documents may come from teaching and research institutions in France or abroad, or from public or private research centers.

L'archive ouverte pluridisciplinaire **HAL**, est destinée au dépôt et à la diffusion de documents scientifiques de niveau recherche, publiés ou non, émanant des établissements d'enseignement et de recherche français ou étrangers, des laboratoires publics ou privés.

An agent-based model of vibration-induced intimal hyperplasia

Maha Reda^{1,2}, Christophe Noël^{1*}, Nicla Settembre³, Jérôme Chambert², Arnaud Lejeune², Gwenaël Rolin^{4,5}
and Emmanuelle Jacquet²

¹Electromagnetism, Vibration, Optics Laboratory, Institut National de Recherche et de Sécurité (INRS), Vandœuvre-lès-Nancy, France.

²Department of Applied Mechanics, Univ. Bourgogne Franche-Comté, FEMTO-ST Institute, UFC/CNRS/ENSMM/UTBM, Besançon, France.

³Department of Vascular Surgery, Nancy University Hospital, University of Lorraine, Vandœuvre-lès-Nancy, France.

⁴Inserm Centre d'Investigation Clinique-1431 (Inserm CIC-1431), Centre Hospitalier Régional Universitaire de Besançon, Besançon, France.

⁵Inserm UMR1098, RIGHT Interactions Greffon-Hôte-Tumeur/Ingénierie Cellulaire et Génique, Etablissement Français du Sang en Bourgogne Franche-Comté, Université de Bourgogne Franche-Comté, Besançon, France.

*Corresponding author(s). E-mail(s): christophe.noel@inrs.fr;

Abstract

Acute exposure to hand-arm transmitted vibrations (HAVs) may decrease the Wall Shear Stress (WSS) exerted by the blood flow on the arterial endothelium. In the case of chronic exposure to HAVs, these WSS changes can lead to arterial growth and remodeling potentially induced by an intimal hyperplasia phenomenon. Accordingly, we implemented an agent-based model (ABM) that captures the hemodynamics-driven and mechanoregulated cellular mechanisms involved in vibration-induced intimal hyperplasia. Our ABM was combined with flow loop experiments that investigated the WSS-modulated secretion of the Platelet-Derived

Growth Factor BB (PDGF-BB) by the endothelial cells (ECs). The ABM rules parameters were then identified and calibrated using our experimental findings and literature data. The model was able to replicate the basal state (no vibration) as well as predict a 30% stenosis resulting from a chronic drop of WSS values mimicking exposure to vibration during a timeframe of 10 years. The study of the influence of different WSS-modulated phenomena on the model showed that the magnitude of stenosis largely depends on the migratory effects of PDGF-BB and the mitogenic effects of Transforming Growth Factor β (TGF- β) on the Smooth Muscle Cells (SMCs). The results also proved that the fall in circumferential stress due to arterial layer thickening to a great extent accounts for the degradation of the Extracellular Matrix (ECM) in the media.

Keywords: Hand-arm vibration, Intimal hyperplasia, Agent-based model, Wall shear stress

1 Introduction

Vibration-induced Raynaud's syndrome is a vascular disorder that may affect workers regularly exposed to Hand-Arm transmitted Vibrations (HAVs) (Brammer et al, 1987; Ashe and Williams, 1964). These high frequency vibrations (40 to 500 Hz) are typically generated by hand-held rotating machines such as drills, jackhammers and grinders (Brammer and Pitts, 2012; Welsh, 1980). In addition to vascular disorders, workers exposed to HAVs may potentially experience numbness and tingling in fingers which lead to the inability to manipulate machines. On an anatomical scale, Raynaud's syndrome may be characterized by arterial stenosis, likely induced in part by an intimal hyperplasia phenomenon (Okada et al, 1987; Takeuchi et al, 1986). Studies suggested that hyper-activation of the sympathetic nervous system, observed in workers exposed to HAVs, may decrease the blood flow in both vibrated and non-vibrated digital arteries (Welsh, 1980; Bovenzi and Griffin, 1997). Consequently, the drop in blood flow may also induce a decrease in Wall Shear Stress (WSS) exerted by the blood on arterial endothelium. Indeed, it has been shown that acute exposure to HAVs reduced WSS in digital arteries (Curry et al, 2002; Noël and Settembre, 2022). Hemodynamic forces, such as WSS specifically, play a significant role in arterial growth and remodeling through the regulation of the endothelium functions (Epstein et al, 1994; Nerem et al, 1998). Indeed, Low Shear Stress (LSS) can promote the endothelial secretion of many mitogenic and chemotactic agents, such as Platelet-Derived Growth Factors (PDGF) (Hsieh et al, 1991; Heydarkhan-Hagvall et al, 2006). These agents may control the proliferation and migration of Smooth Muscle Cells (SMCs) as well as the dynamics of the Extracellular Matrix (ECM), which are all relevant mechanisms involved in the intimal hyperplasia phenomenon (Minion et al, 2000; Li et al, 2011; Koyama et al, 1994; Newby and Zaltsman, 2000). In addition to the effects of WSS on the endothelium, changes within

the stress and strain fields in the arterial tissues due to the growth or reduction of arterial layers were also proven to induce SMCs mechanotransduction at the cellular level (Kona et al, 2009; Bayer et al, 1999). Consequently, a multiscale mechanobiological framework was set up to understand this multifactorial disorder and its manifestation on different spatial and temporal scales Noël et al (2022).

To this end, different approaches were developed previously for modeling the emergence of various pathologies in vascular systems. For example, continuum-based models and mathematical formulations based on Partial Differential Equations (PDE) allow the multiscale modelling of biological mechanisms and were used extensively to study stress-induced arterial growth (Kuhl et al, 2007; Menzel, 2007; Rodriguez et al, 1994) and hemodynamic-driven neointimal hyperplasia in vein grafts (Donadoni et al, 2017). Constrained Mixture Models (CMMs) in which various arterial constituents are modeled with different behaviors and turnover rates, were also developed to model arterial growth and remodeling in response to hemodynamic stimuli (Humphrey and Rajagopal, 2002; Horvat et al, 2019) or hypertension (Gleason and Humphrey, 2004). While these techniques offer a multiscale view of the arterial growth, they fall short of capturing the discrete nature of the biological processes occurring at the cellular level. Therefore, Agent-Based Models (ABMs) are attracting a particular interest in an attempt to overcome this drawback. With their ability to model vascular cells as individual agents that behave and interact according to a set of predefined rules, ABMs represent a suitable tool for simulating biological behaviors in vascular pathologies (Thorne et al, 2011; Evans et al, 2008; Boyle et al, 2010). Furthermore, ABMs can be coupled with continuum-level models such as Finite Element Models (FEMs) offering a multiscale mechanobiological approach capable of tackling the mechanoregulation and hemodynamic modulation of individual-based vascular dynamics (Zahedmanesh and Lally, 2012; Rouillard and Holmes, 2014). For instance, Keshavarzian et al (2018) used a fully coupled ABM-FEM model to study arterial behavior at the cellular level, in response to transient increases in blood pressure. Moreover, Corti et al (2020) coupled an ABM with a computational fluid dynamics model to simulate hemodynamic-driven plaque formation during atherosclerosis. This combination between continuum and discrete methods provided a deeper multiscale understanding of biological mechanisms and their driving factors.

Within this framework, the parametrization of the biological mechanisms involved is a crucial step in building an ABM that can provide realistic insights into the phenomena modeled. The ABM parameters can be determined experimentally or identified using literature data (Thorne et al, 2007; Garbey et al, 2015). In addition, ABMs offer the possibility of modeling several mechanisms of certain components of the biological system separately. When combined together, all these mechanisms produce the complex behavior of the whole system (Thorne et al, 2011). By characterizing complex processes by separate

individual ones, ABMs are able to capture the most influential parameters and mechanisms involved in the emergence of pathologies and patterns.

Up to now, few studies have attempted to model the secretion of factors by ECs which regulates SMC dynamics and possibly leads to the onset of intimal hyperplasia (Donadoni et al, 2017). Modeling WSS-modulated and mechanoregulated factor secretion could give new insights on pertinent contributors to intimal hyperplasia. Therefore, we present herein an on-lattice ABM that includes hemodynamic-driven and mechanoregulated biological mechanisms involved in the vibration-induced intimal hyperplasia phenomenon. We added the mitogenic effects of the WSS-modulated Transforming Growth Factor β (TGF- β), the migratory effects of PDGF-BB on SMCs, and the effects of Nitric Oxide (NO) on SMCs apoptosis, to existing ABMs. The model was coupled with in-vivo experiments that helped in identifying the equation parameters of the PDGF-BB secretion rate by ECs. Finally, we studied the effects of each WSS-modulated factor on the model's behavior to determine pertinent contributors to the onset of vibration-induced intimal hyperplasia.

In our model, starting from a healthy artery, a uniform profile of WSS was applied on the endothelium. The WSS values were chosen to mimic the absence or presence of vibration. The ABM then simulated the cells' response according to these prescribed WSS values, and also generated the change induced in arterial geometry. A regularization method was applied to minimize the inherent geometrical anisotropy of the on-lattice ABM and thus ensure isotropic growth in the case of uniform spatial distribution of WSS (Dardik et al, 2005). The model parameters were partially identified experimentally using our flow loop experiments or derived from literature data. Our model was also coupled with a PDE diffusion module that simulated inside the arterial layers the physical diffusion of certain secreted growth factors involved in intimal hyperplasia. The model was tested under two states: i) the 'No Vibration' state in which no exposure to vibration was simulated and the WSS value was kept physiological during the simulation time, and ii) the 'Vibration' state in which the physiological WSS value was perturbed by regular drops replicating the daily working condition of workers exposed to HAVs (Noël and Settembre, 2022). The influence of WSS-modulated biological mechanisms involved in our ABM was assessed and a sensitivity analysis of the PDGF-BB diffusion coefficient performed. Our ABM, which is a part of a more complex ABM-FEM framework, will be used to predict long-term arterial growth during chronic exposure to vibration.

2 Materials and Methods

2.1 Agent-based model

The ABM was implemented in NetLogo 6.0.4 (Wilensky, 1999) and simulated the cellular mechanisms involved in the onset of vibration-induced intimal hyperplasia. Starting from a healthy artery with an initial circular geometry, a spatially uniform physiological WSS profile was applied on the endothelium.

Intimal hyperplasia was induced by a decrease in these WSS values mimicking exposure to vibration. The ABM was implemented in an iterative process ($k = 0, 1, \dots, K$) as follows: i) a constant duration T was chosen for one iteration k where the WSS value was kept constant at a value matching the exposure condition we wanted to simulate, ii) all the biological mechanisms of the ABM were computed for T , iii) the artery geometry and behavior were updated at each iteration k . This process was iterated K times such that $K \times T = T_{\text{end}}$ where T_{end} is the total time of the simulation (Figure 1). This total simulation time matched the average duration of the careers of workers exposed to HAVs (Donati et al, 2008). Therefore, at each ABM iteration $k = 0, 1, \dots, K$ of duration T , the cell dynamics were simulated based on a set of behavioral rules modulated by the WSS value (matching the absence or presence of vibration exposure) as well as the circumferential stress field values resulting from applying physiological pressure on the inner wall of the artery. Finally, after each iteration, a geometrical regularization was applied to limit the numerically-induced anisotropy (the stage of boundary smoothing in Figure 1). Due to the stochastic nature of certain mathematical equations describing the biological mechanisms used in our ABM (e.g. SMCs proliferation and migration probabilities), all the output values presented hereafter were calculated as the average of N simulations, where N was chosen as a trade-off between the minimization of errors (margins between the final SMCs and Collagen counts of simulations in the 'No Vibration' state and their basal values) and computational cost. The ABM was controlled by Python scripts using the PyNetLogo package which offers flexibility and advanced analysis capabilities (Jaxa-Rozen and Kwakkel, 2018).

2.1.1 ABM building and initialization

A 2D arterial geometry was drawn in a $< 110 \times 110 >$ square lattice, with internal (r_i) and external (r_e) radii of 400 μm and 500 μm respectively (Noël and Settembre, 2022). Each lattice site of dimension 10 $\mu\text{m} \times 10 \mu\text{m}$ can be occupied by only one of the three agent types used in our model: Endothelial Cells (ECs), SMCs and ECMs. The model consisted of a monolayer of ECs composing the intima and multiple layers of SMCs and ECMs making up the media. The number of ECs corresponded to the number of patches making up a single layer at a radius $r_i = 400 \mu\text{m}$ ($N_{\text{EC}} = 228$ cells). SMCs made up 68% of the media while 32% were occupied by ECMs (Todd et al, 1983). This resulted in 1770 SMCs and 834 ECMs. The intima and the media layers were separated by the internal elastic lamellae (IEL) (Figure 2). SMC and EC diameters were assumed to be identical and fixed at 10 μm (Todd et al, 1983), corresponding to our mesh dimension of 10 μm . ECM agents were labeled by either collagen (C) or elastin (E) with a C/E ratio of 3.12 (Fischer and Llaurodo, 1966). Thus, each ECM patch could be occupied exclusively by either collagen or elastin. Consequently, the ECM was made up of 625 patches containing collagen and 209 patches containing elastin. Moreover, the total initial mass of collagen was calculated by multiplying the initial collagen mass per SMC (3.1×10^{-4}

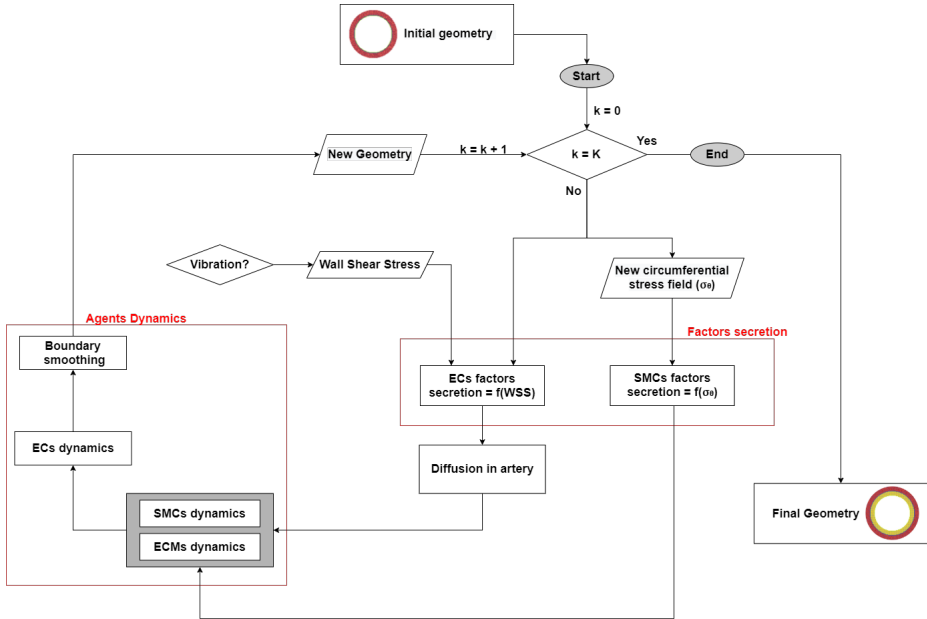


Fig. 1 Simulation flowchart showing the iteration process inside the ABM

$\mu\text{g}\cdot\text{cell}^{-1}$ (Zahedmanesh and Lally, 2012)) with the number of SMCs at $k = 0$. The total elastin mass was retrieved from the C/E ratio. Consequently, at $k=0$ each ECM agent was assigned an individual mass (m_c for collagen and m_e for elastin) derived from uniformly distributing the total initial masses of collagen and elastin among total collagen or elastin patches, respectively ($m_c = 0.86$ ng and $m_e = 0.86$ ng). Each lattice site, or patch, was also assigned a characteristic (i.e., type) corresponding to its position inside the artery: intima, media, elastic lamellae, lumen and boundary. Each patch has the ability to update its type according to the new emerging geometry. For example, a lumen patch can become an intima patch after intimal thickening. Agents and patches were assigned a set of predefined behaviors based on their type. The agents' dynamics inside the ABM were based on empirical rules (probabilistic or not) derived from literature and our own experimental tests. The agents' mechanisms and their corresponding mathematical equations are detailed in Appendix A. The model was initialized in the physiological state (WSS = 3 Pa) and then perturbed by a drop in the WSS values from 3 Pa to 1 Pa, matching exposure to vibration (Noël and Settembre, 2022).

2.1.2 Development of ABM rules

ECs secretory rules

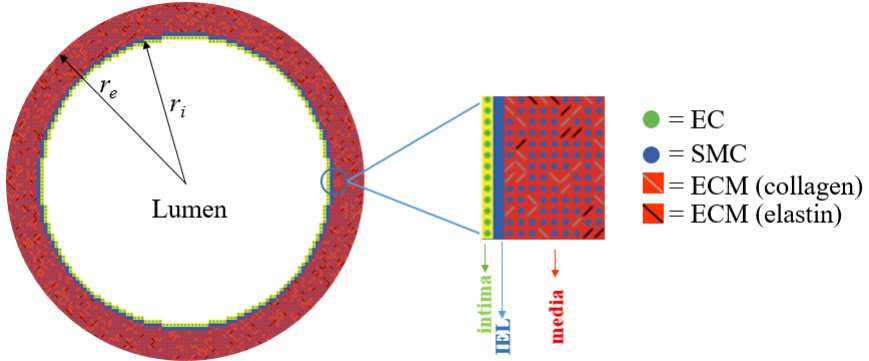


Fig. 2 ABM view of the constructed 2D section of a muscular artery showing the intima (yellow) and media (red) layers separated by the internal elastic lamellae (IEL) (blue) and their Cell/ECM contents

WSS modulates the secretion of endothelium-derived Growth Factors (GFs), such as PDGF-BB and TGF- β , and relaxing factors such as Nitric Oxide (NO) (Hsieh et al, 1991; Ohno et al, 1995; Andrews et al, 2010). These factors then diffuse in the arterial tissue and modulate SMC dynamics. In our model, a uniform value of WSS (τ) was applied on the endothelium composed of ECs. The EC-secretion of the different factors as a function of WSS was modelled using mathematical formulations derived from the literature and our experimental data.

For instance, ECs secrete high levels of PDGF-BB when exposed to low values of WSS (Hsieh et al, 1991). In order to identify the parameters of the mass production rate of the EC-secreted PDGF-BB i.e., $\dot{m}_{\text{PDGF-BB}}^{\text{EC}}(\tau)$ (Table A1), we conducted flow loop experiments to determine the mass of PDGF-BB secreted per each EC when exposed to two values of WSS: 1 Pa and 3 Pa (see section 2.3). The PDGF-BB masses for 1 Pa and 3 Pa obtained from our experiments were then combined with experimental data from Hsieh et al (1991) of PDGF-BB mRNA levels for WSS values ranging from 0 to 5 Pa. The PDGF-BB masses corresponding to each WSS value, other than 1 and 3 Pa, were then obtained by rules of proportionality. The values were previously recalibrated by a vertical translation at 3 Pa, assuming no PDGF-BB secretion for the basal state of 3 Pa (Sjölund et al, 1988). Finally, these data were fitted to the mathematical formulation expressed as follows:

$$\begin{aligned} \dot{m}_{\text{PDGF-BB}}^{\text{EC}}(\tau) = & \alpha Q_{\text{PDGF-BB}}^1 (1 - \exp(-(\tau - \tau_{\text{phys}})/\kappa_{\text{PDGF-BB}}^1)) \\ & + Q_{\text{PDGF-BB}}^2 (1 - \exp((\tau - \tau_{\text{phys}})/\kappa_{\text{PDGF-BB}}^2)) \\ & + q_{\text{PDGF-BB}}(\tau - \tau_{\text{phys}}) \end{aligned} \quad (1)$$

8 *An agent-based model of vibration-induced intimal hyperplasia*

where $0.6 \leq \tau \leq 3$ Pa, $\tau_{\text{phys}} = 3$ Pa, $\alpha = -1$, $Q_{\text{PDGF-BB}}^1 = 5.44 \times 10^{-5}$ fg·s⁻¹, $\kappa_{\text{PDGF-BB}}^1 = 1$ Pa, $Q_{\text{PDGF-BB}}^2 = 5.15 \times 10^{-4}$ fg·s⁻¹, $\kappa_{\text{PDGF-BB}}^2 = 1$ Pa and $q_{\text{PDGF-BB}} = 2.94 \times 10^{-4}$ fg·s⁻¹·Pa⁻¹.

Likewise, the secretion of TGF- β is also modulated by the WSS values. The rule of the EC-secreted TGF- β mass production rate was fitted using literature data (Cucina et al, 1998; Ohno et al, 1995):

$$\dot{m}_{\text{TGF-}\beta}^{\text{EC}}(\tau) = Q_{\text{TGF-}\beta} + q_{\text{TGF-}\beta} \times \tau \quad (2)$$

where $Q_{\text{TGF-}\beta} = 4.26 \times 10^{-4}$ fg·s⁻¹, $q_{\text{TGF-}\beta} = 4.26 \times 10^{-4}$ fg·s⁻¹·Pa⁻¹ and τ is the WSS value in Pa.

In addition, the secretion of the endothelium-derived relaxing factor NO was also implemented in our ABM as a function of the WSS values. Due to its high diffusion coefficient ($D_{\text{NO}} = 3.33 \times 10^{-5}$ cm²·s⁻¹ (Kanai et al, 1995)), the NO steady-state molar concentration was rapidly reached (150 s (Andrews et al, 2010)). Consequently, in our ABM we modeled the global steady-state molar concentration of NO using experimental data retrieved from Andrews et al (2010):

$$C_{\text{NO}}^{\text{EC}}(\tau) = C_1(1 - \exp(-\tau/\kappa_{\text{NO}})) + C_2 \quad (3)$$

where $C_1 = 51.7 \times \Delta h$ in nM, $\kappa = 0.95$ Pa, $C_2 = 20.22 \times T$ in nM and T in hours. nM stands for 10⁻⁹ mol.l⁻¹.

GFs diffusion

In order to model the diffusion of the growth factors through the artery layers, our ABM was coupled with a finite difference model developed with Python scripts that solves the diffusion equation:

$$\frac{\partial m_{\text{GF}}^{\text{EC}}(\mathbf{x}, t)}{\partial t} = D_{\text{GF}} \nabla^2 m_{\text{GF}}^{\text{EC}}(\mathbf{x}, t) + f(\mathbf{x}, t) \quad (4)$$

where $m_{\text{GF}}^{\text{EC}}(\mathbf{x}, t)$ is the mass of the GFs (PDGF-BB and TGF- β) at location $\mathbf{x} = (x, y)$ inside the artery and time $t \in [0, T]$, ∇^2 denotes the Laplacian with respect to \mathbf{x} , D_{GF} the constant diffusion coefficient inside the artery, and $f(\mathbf{x}, t)$ the source term describing the continuous factors secretion by the ECs (Watson et al, 2020). Each EC was considered as a point source of PDGF-BB and TGF- β with a constant mass production rate $\dot{m}_{\text{GF}}^{\text{EC}}(\tau)$ (Table A1). Consequently, the source term $f(\mathbf{x}, t)$ corresponded to the summation of all the N_{EC} point sources at EC location $\xi_{\mathbf{i}, \mathbf{i}=1, \dots, N_{\text{EC}}}$:

$$f(\mathbf{x}, t) = \dot{m}_{\text{GF}}^{\text{EC}} \sum_{\mathbf{i}=1}^{N_{\text{EC}}} \delta(\mathbf{x} - \xi_{\mathbf{i}}) \quad (5)$$

where $\delta(\mathbf{x} - \xi_{\mathbf{i}})$ is the Dirac distribution in two-dimensional space. The diffusion equations for PDGF-BB and TGF- β were solved at each ABM iteration k for 0

$\leq t \leq T$. At $t = T$, the final mass map of GFs was communicated to the ABM. Subsequently, at each iteration $k = 1, \dots, K$ initial conditions introduced in the diffusion model at $t = 0$ (${}^k m_{\text{GF}}^{\text{EC}}(\mathbf{x}, 0)$) correspond to the final mass map ($t = T$) retrieved from the diffusion model at the previous iteration (${}^{k-1} m_{\text{GF}}^{\text{EC}}(\mathbf{x}, h)$):

$${}^k m_{\text{GF}}^{\text{EC}}(\mathbf{x}, 0) = {}^{k-1} m_{\text{GF}}^{\text{EC}}(\mathbf{x}, h) \quad k = 1, \dots, K \quad \forall \mathbf{x} \quad (6)$$

$${}^0 m_{\text{GF}}^{\text{EC}}(\mathbf{x}, 0) = \begin{cases} 0 & \text{if GF} = \text{PDGF-BB} \\ {}_{\text{phys}} m_{\text{TGF-}\beta}^{\text{EC}}(\mathbf{x}) & \text{if GF} = \text{TGF-}\beta \end{cases} \quad (7)$$

where ${}^0 m_{\text{GF}}^{\text{EC}}(\mathbf{x}, 0)$ is the mass distribution of the GF at $k = 0$ and ${}_{\text{phys}} m_{\text{TGF-}\beta}^{\text{EC}}(\mathbf{x})$ is the physiological mass distribution of TGF- β diffused by ECs and obtained from a preliminary computation. The EC coordinates (ξ_i), the artery dimensions and boundaries were updated in the ABM and communicated to the diffusion model at each iteration. GFs diffusing inside the lumen ($\|\mathbf{x}\| \leq r_i$, $\|\mathbf{x}\|$ is the Euclidean norm of \mathbf{x}) were considered to be immediately flushed by the blood flow (Thorne et al, 2011). Therefore, the condition $m_{\text{GF}}^{\text{EC}}(\mathbf{x}, t) = 0$ for $\|\mathbf{x}\| \leq r_i$ was applied to model this behavior.

For the external boundary condition two cases were considered: i) a full closed medium condition simulating a no flux boundary condition applied on the external boundary at radius r_e of the media layer $\nabla m(\mathbf{x}, t) = 0$ for $\|\mathbf{x}\| = r_e$ where ∇ denotes the gradient; ii) an infinite medium by taking into account the surrounding tissue around the artery in the diffusion model. The diffusion coefficients of the different factors used in the model are given in Table B5.

SMCs dynamics

The biological behavior of the SMCs (SMCs dynamics) implemented in our ABM includes the SMC-secretion of soluble factors, the proliferation/apoptosis of the SMCs and their migration from the media to the intima. First, the vibration-induced decrease in WSS values upregulates the activated MMP-2 (Matrix Metalloproteinase-2) levels secreted by the SMCs (Garanich et al, 2005; Sakamoto et al, 2006). MMP-2 are involved in ECM degradation that can facilitate the migration of SMCs from the media to the intima during intimal hyperplasia. The SMC-secretion rule of activated MMP-2 as a function of WSS was derived from literature data (Sakamoto et al, 2006; Garanich et al, 2005) and expressed as follows:

$$m_{\text{MMP-2}}^{\text{SMC}}(\tau) = M_{\text{MMP-2}}^1 (\exp(-(\tau - \tau_{\text{phys}})/\kappa_{\text{MMP-2}}^1) - 1) \quad (8)$$

where $\tau_{\text{phys}} = 3$ Pa, $M_{\text{MMP-2}}^1 = 2.66 \times 10^{-5} \times T$ in fg, $\kappa_{\text{MMP-2}}^1 = 1$ Pa and T in hours.

In addition, the SMC-secretion of GFs and MMP is also modulated by mechanical stress. For instance, high circumferential stress values enhance TGF- β , PDGF-BB, MMP-9 and MMP-2 secretion by SMCs (Keshavarzian

et al, 2018). MMP-2 levels are also upregulated by low circumferential stress values. The mechanoregulated SMC-secretion rules are detailed in Table A2.

The proliferation rule of SMCs was expressed in terms of a probability and applied on each SMC agent at each ABM iteration k . The SMCs possess a basal proliferation probability to which were added the proliferative effects of the total PDGF-BB mass secreted by the ECs and SMCs, and the EC-secreted TGF- β mass. The final proliferation probability of one SMC per one timestep is expressed by the equation below:

$$\mathcal{P} = \mathcal{P}_{\text{basal}} + \mathcal{P}_{\text{PDGF-BB}} + \mathcal{P}_{\text{TGF-}\beta} \quad (9)$$

where $\mathcal{P}_{\text{basal}} = 1.46 \times 10^{-4}$ (Chapman et al, 2000).

Studies have shown that PDGF-BB is a mitogen for SMCs that can increase their proliferation probability when secreted in the artery due to low WSS values, resulting in arterial growth (Wolf et al, 2005; Li et al, 2011). However, in the case of decreased wall tension, the atrophic remodeling of the arterial wall is observed (Bayer et al, 1999). In order to model this phenomenon, we added a correcting factor modulated by circumferential stress that acts on each SMC site to reduce the effects of EC-secreted PDGF-BB on SMC proliferation probability (Table A2). Consequently, the proliferation probability of one SMC as a function of PDGF-BB is expressed in our ABM as:

$$\mathcal{P}_{\text{PDGF-BB}} = A_{\text{PDGF-BB}}^1 (1 - \exp(-m_{\text{PDGF-BB}}/\omega_{\text{PDGF-BB}}^1)) + \alpha A_{\text{PDGF-BB}}^2 \times m_{\text{PDGF-BB}} \quad (10)$$

where $A_{\text{PDGF-BB}}^1 = 2.32 \times 10^{-2}$, $m_{\text{PDGF-BB}} = m_{\text{PDGF-BB}}^{\text{SMC}}$ (Table A2) + $m_{\text{PDGF-BB}}^{\text{EC}}$ (from diffusion) + $C_f \times m_{\text{unit}}$ (Table A2) in fg, $\omega_{\text{PDGF-BB}}^1 = 4.33$ fg, $\alpha = -1$, $A_{\text{PDGF-BB}}^2 = 3.35 \times 10^{-6}$ and $m_{\text{unit}} = 1$ fg.

In contrast, TGF- β can act as a mitogen to SMCs only when present in low levels. This is due to the fact that a physiological level of TGF- β is essential in maintaining a contractile phenotype of SMCs and ensuring a physiological state (Cucina et al, 1998). In our model, when the WSS values decrease with exposure to vibration, the EC-secretion of TGF- β decreases. Thus, the mass of TGF- β ($m_{\text{TGF-}\beta}$) present around the SMC and obtained from diffusion through the artery would decrease. Therefore, the SMCs proliferation probability would increase according to the following rule:

$$\mathcal{P}_{\text{TGF-}\beta} = A_{\text{TGF-}\beta} \exp(-m_{\text{TGF-}\beta}/\omega_{\text{TGF-}\beta}) \quad (11)$$

where $A_{\text{TGF-}\beta} = 2.94 \times 10^{-4}$, $m_{\text{TGF-}\beta} = m_{\text{TGF-}\beta}^{\text{SMC}}$ (Table A2) + $m_{\text{TGF-}\beta}^{\text{EC}}$ (from diffusion) in fg and $\omega_{\text{TGF-}\beta} = 10^{-3}$ fg.

In addition, we modeled the effects of NO molar concentration on SMC apoptosis probability (\mathcal{A}). When the NO molar concentrations decrease with the drop of WSS values, SMCs apoptosis probability also decrease (Krick et al, 2002; Nishio et al, 1996). The rule parameters were derived from literature data and readjusted to our model's basal apoptosis probability ($\mathcal{A}_{\text{basal}}$) (Chapman

et al, 2000; Krick et al, 2002):

$$\mathcal{A} = \mathcal{A}_{\text{basal}} + \mathcal{A}_{\text{NO}} \quad (12)$$

$$\mathcal{A}_{\text{NO}} = \gamma_{\text{NO}} \times (C_{\text{NO}}^{\text{EC}} - {}^{\text{phys}}C_{\text{NO}}^{\text{EC}}) \quad (13)$$

where $\mathcal{A}_{\text{basal}} = 1.46 \times 10^{-4}$, $\gamma_{\text{NO}} = 7.31 \times 10^{-7} \text{ nM}^{-1}$ and ${}^{\text{phys}}C_{\text{NO}}^{\text{EC}} = 69.7 \text{ nM}$.

In the basal conditions, SMCs apoptosis and proliferation probabilities were set as equal to ensure the physiological state (no vibration):

$$\mathcal{A}_{\text{basal}} = \mathcal{P}_{\text{basal}} \quad (14)$$

Given that the proliferation and apoptosis of SMCs were built on probabilities, at each iteration an event assessment must be carried out to determine which event an SMC has to undergo. Consequently, at each iteration k , a random number p between 0 and 1 is generated. If $p \leq \mathcal{P}$, the SMC undergoes proliferation, which means that the SMC divides into two daughter cells. In our numerical model, when an SMC underwent proliferation, a new daughter cell was created randomly on one of the empty adjacent patches (neighbors) of the proliferating SMC. If no empty neighbor was found, the daughter cell would push one of the surrounding cells along the shortest path to an empty patch and the new daughter cell would be positioned inside the newly created empty neighbor. In contrast, if $p \leq (1 - \mathcal{A})$, the SMC undergoes apoptosis, which means that the SMC dies and is removed from the model. Finally, the remaining SMCs would be rearranged following paths of minimal energy to fill the empty patch left by the apoptotic cell (Corti et al, 2020).

During intimal hyperplasia, SMC migration from the media to the intima is modulated by EC-secreted PDGF-BB mass (Palumbo et al, 2002). In our model, we assumed that only PDGF-BB secreted by the ECs can act in a paracrine manner to stimulate chemotaxis (Dardik et al, 2005). When the migration is activated, the SMCs then undergo chemotactic migration from the media to the intima along an increasing gradient of PDGF-BB concentrations. The migration rule was expressed as a probability (\mathcal{M}) and derived from literature data (Dardik et al, 2005; Bornfeldt et al, 1994) as follows:

$$\mathcal{M} = A_{\text{PDGF-BB}} (1 - \exp(-m_{\text{PDGF-BB}}^{\text{EC}} / \omega_{\text{PDGF-BB}})) \quad (15)$$

$A_{\text{PDGF-BB}} = 7.91 \times 10^{-4}$, $m_{\text{PDGF-BB}}^{\text{EC}}$ (from diffusion) in fg and $\omega_{\text{PDGF-BB}} = 4.9 \times 10^{-2}$ fg. Numerically, once the migration is activated, the SMCs started moving towards the intima by discrete steps, to mimic chemotaxis acitvated by the PDGF-BB mass gradient. Since the length of one patch is 10 μm in our model, the resulting migration speed was 10 $\mu\text{m}\cdot\text{h}^{-1}$ which is consistent with the SMC migration speed calculated by DiMilla et al (1993). Once they reached the intima, the SMCs stopped migrating and their movement could only be due to pressure from other SMCs (Gerthoffer, 2007). In addition to chemotaxis, SMCs migration may also be induced by durotaxis, where SMCs movement is modulated by the ECM rigidity gradient inside the arterial wall (Isenberg et al, 2009). However, durotaxis was not considered in our current model.

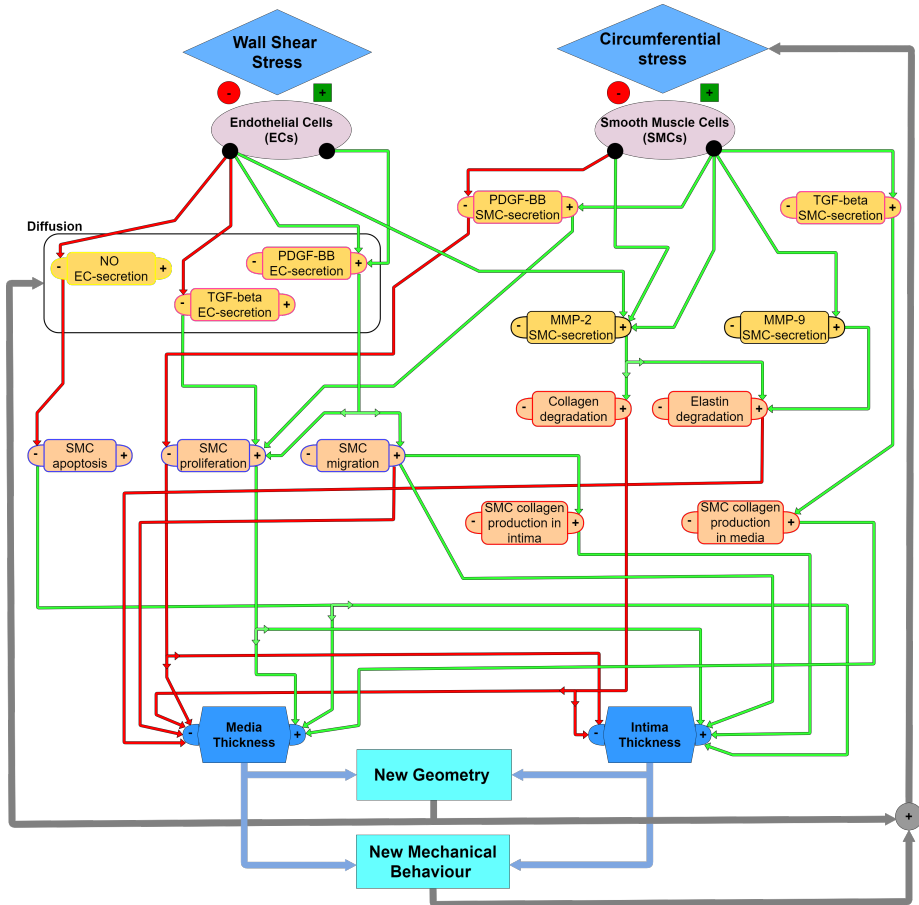


Fig. 3 Biological mechanisms and their interactions occurring inside the ABM. Green lines indicate an enhanced manifestation of the biological mechanism at the end of the arrow while red lines indicate a diminished one

ECMs dynamics

SMCs are responsible for ECM production. Indeed, collagen production can be modeled as a given mass secreted by one SMC per hour ($m_c = 8.99 \text{ fg} \cdot \text{h}^{-1} \cdot \text{cell}^{-1}$ (Zahedmanesh and Lally, 2012)). By assigning an initial mass of one collagen patch present in the ABM ($m = 0.84 \text{ ng}$), we calculated the synthesis probability of collagen as the inverse of time taken by one SMC to create one collagen patch. During the physiological state, basal collagen degradation ($\mathcal{D}_{\text{basal}}^c$) and synthesis ($\mathcal{S}_{\text{basal}}^m$) probabilities in the media layer were set to be equal:

$$\mathcal{S}_{\text{basal}}^m = \mathcal{D}_{\text{basal}}^c = 1.07 \times 10^{-5} \quad (16)$$

In contrast, due to its long half-life (Humphrey and Rajagopal, 2002), the basal production and basal elimination of elastin were not modeled.

Furthermore, SMC-secreted MMP-2 and MMP-9 can modulate the SMCs probability of collagen degradation and also induce elastin degradation. The degradation of collagen by SMCs as a function of MMP-2 was derived from the value of the collagen mass degraded by a given mass of MMP-2 (410 pg collagen/pg MMP-2/h (Zahedmanesh and Lally, 2012)). Similar to basal collagen synthesis probability, the collagen degradation modulated by MMP-2 was calculated as the inverse of time taken by a given mass of MMP-2 to degrade one patch of collagen. The collagen degradation probability as a function of MMP-2 was expressed as follows:

$$\mathcal{D}_{\text{MMP-2}}^c = \gamma_{\text{MMP-2}}^1 \times m_{\text{MMP-2}} \quad (17)$$

where $\gamma_{\text{MMP-2}}^1 = 3.5 \times 10^{-4} \text{ fg}^{-1}$, $m_{\text{MMP-2}} = m_{\text{MMP-2}}^{\text{SMC}}(\tau) + m_{\text{MMP-2}}^{\text{SMC}}(\sigma_\theta)$ in fg.

In addition, MMP-2 and MMP-9 induce the degradation of elastin following the same model but with different slopes, $\gamma_{\text{MMP-2}}^2 = 3.14 \times 10^{-6} \text{ fg}^{-1}$ and $\gamma_{\text{MMP-9}} = 1.04 \times 10^{-6} \text{ fg}^{-1}$ for MMP-2 and MMP-9 respectively (Table A4).

Moreover, the phenotypic modulation of SMCs from a contractile to a synthetic phenotype results in an increased secretion of collagen. In order to take this mechanism into account, we assumed that the SMCs changed into a synthetic phenotype when they reached the intima (Okada et al, 1987; Sjölund et al, 1986). Consequently, the basal production probability of collagen in the intima is higher than that in the media, while the basal degradation probability remained unchanged:

$$\mathcal{S}_{\text{basal}}^i = 2.24 \times 10^{-5} \quad (18)$$

All the biological phenomena implemented and their interactions are detailed in Figure 3.

2.1.3 Geometrical regularization

Discrete cell movements inside the artery can create geometrical spikes (breaking the continuous endothelium) at the boundaries, especially at the lumen interface, which can compromise the axisymmetric geometry of the model and produce non-biological shapes (Corti et al, 2020). Consequently, in order to ensure the compact structure of the model, a smoothing algorithm was applied on the interfaces after each iteration. It consists in: i) calculating an average radius of the interface, ii) searching for cells that have a distance to the center less than (for internal boundaries) or greater than (for external boundary) the average radius of the interface, and iii) rearranging the cells by moving them to the closest empty patch at the interface in a way that increases the contact surface between them. In addition, the model takes into account the movement of the internal elastic lamellae (IEL) between the media and the intima. In the case of medial growth, proliferating SMCs or ECM agents can

push the IEL patches towards the lumen center without crossing to the intima (the migrating SMCs are able to pass through the IEL).

2.2 Model assessment under 'No Vibration' state and during a chronic exposure to vibration

The ABM was tested under the 'No Vibration' state ($\tau = 3$ Pa) in order to ensure its stability, i.e., no significant change in SMC or ECM number should be observed. In addition, due to the stochastic nature of the ABM, a sensitivity analysis was performed to quantify the influence of the number of simulations (N) on the equilibrium. More precisely, assuming that the values maintain their basal levels in time in the absence of vibration, we evaluated the errors on the final SMCs and collagen counts relative to their basal counts. N was chosen as the number of simulations after which the relative errors on SMCs and collagen counts remained stable.

During exposure to vibration, the WSS values fell to 1 Pa. In our case study, the model was tested for a duration of 4 hours of vibration exposure per day, corresponding to the condition of workers having an exposure time of more than 20 hours per week and are more likely to develop vibration-induced intimal hyperplasia on the long term (Donati et al, 2008; Bovenzi et al, 1985). In addition, in our model, the WSS value of 1 Pa which mimics vibration exposure, remained constant throughout the 4 hours, assuming no change in WSS occurs during vibration exposure time. A simulation time of 10 years was chosen, as it represents the number of years' exposure before the onset of vibration-induced intimal hyperplasia (Ashe and Williams, 1964; EN NF ISO 5349-1:2001, 2002). A sensitivity analysis of the PDGF-BB diffusion parameter ($D_{\text{PDGF-BB}}$) was conducted by increasing or decreasing $D_{\text{PDGF-BB}}$ by one order of magnitude (a factor of 10). Moreover, the choice of boundary conditions (BCs) in the GF diffusion models was studied by comparing two theoretical cases: i) an infinite 2D plane assuming that the GFs diffused outside the arterial wall, and ii) a no flux boundary on the external boundary of the media.

The influence of taking into account certain WSS-modulated factors secreted by the ECs and SMCs was also studied. To do this, we compared the full model's behavior to that in the absence of each of the following mechanisms: i) EC-secretion of TGF- β , ii) EC-secretion of NO, and iii) SMC-secretion of MMP-2 (WSS-regulated (Table A1)).

Finally, we assessed the model's behavior by taking into account the effects of the circumferential stress field (hoop stress (σ_θ)) on the cellular mechanisms. Hoop stress values were obtained by assuming a homogeneous thick-walled cylinder and using Lamé's theory with the following analytical model:

$$\sigma_\theta = \frac{Pr_i^2}{r_e^2 - r_i^2} + \frac{r_i^2 r_e^2}{r^2} \left(\frac{P}{r_e^2 - r_i^2} \right) \quad (19)$$

where r_i and r_e are the internal and external radii respectively and P represents the pressure applied on the inner wall of the artery. A physiological inner pressure $P = 13$ kPa was applied on the endothelium at each ABM iteration (Holzapfel et al, 2000).

2.3 Flow loop experiments

In order to assess the model parameters of the PDGF-BB secretion by the endothelial cells, flow loop experiments were conducted on Human Umbilical Vein Endothelial Cells (HUVECs). The aim was to measure the concentrations of the EC-secreted PDGF-BB as a function of two values of Shear Stress (SS): 1 Pa mimicking the presence of vibration, and 3 Pa corresponding to the physiological state.

Cell culture

HUVECs were obtained from PELOBiotech and harvested from 10 human umbilical veins. The ECs were cultured at a density of 2×10^5 cells·cm⁻² and placed in a humidified incubator at 37°C-5% CO₂, with 2% fetal bovine serum (FBS). The culture medium was changed twice a week and the cells were trypsinized and amplified when confluence was reached.

Shear Stress application (Ibidi pump system)

100 μ l suspension of ECs at 0.5×10^6 cells·ml⁻¹ were placed on collagen coated canals of Luer μ -Slide plates and incubated for three days at 37°C-5% CO₂ with the culture medium changed every day. The plates were then connected to the fluidic unit of an Ibidi pump and placed inside an incubator at 37°C-5% CO₂. Finally, the HUVECs were exposed to two values of steady shear stress, 1 Pa or 3 Pa, for 2 hours followed by 2 hours of rest without shear stress. In order to preserve the attachment of the cells to the plates, the shear stress was gradually increased to its target value which was then kept constant until the end of the shear stress application time.

PDGF-BB measurement

100 μ l of Conditioned Medium (CM) was collected after 4 hours (2 hours of shear stress and 2 hours rest) from the shear stress-exposed cells and from the control cells exposed to static conditions. PDGF-BB in the CM was assayed using an enzyme-linked immunosorbent assay (ELISA) kit according to the manufacturer's instructions. The optical density at a wavelength of $\lambda = 450$ nm was measured using a microplate photometer (Thermo Multiskan FC). Moreover, the total number of ECs was assayed at the end of each experiment in order to determine the mass of PDGF-BB secreted by one EC. Finally, statistical analysis was conducted using one-way ANOVA. Fisher's Least Significant Difference (LSD) post-hoc test was then used to find means that are significantly different from each other. A value of $p < 0.05$ was deemed statistically significant.

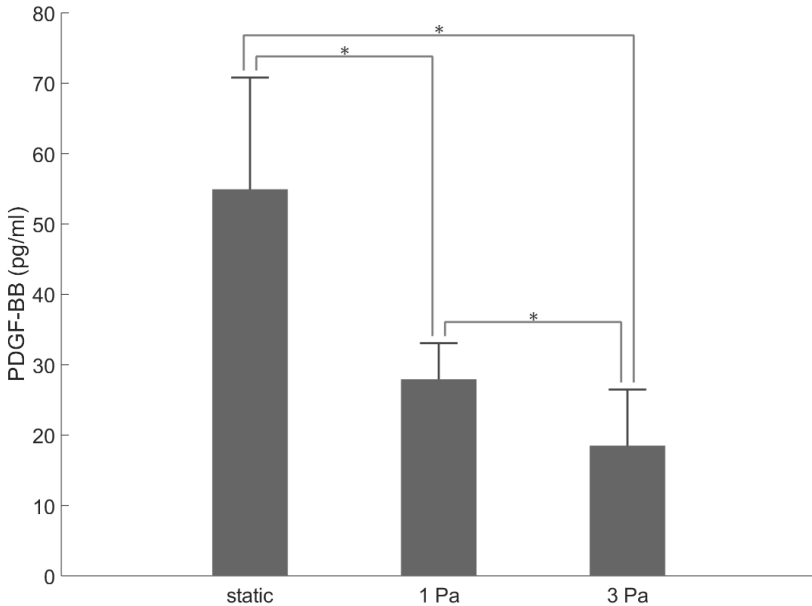


Fig. 4 PDGF-BB concentrations (pg/ml) after 4 hours in static conditions (0 Pa), conditioned medium exposed to low shear stress (1 Pa) and conditioned medium exposed to physiological shear stress (3 Pa). (* $p < 0.05$, by one-way ANOVA followed by Fisher's LSD test). The results are expressed as means \pm Standard Deviation (SD) for $n = 10$ experiments

3 Results

3.1 Low shear stress stimulates the secretion of PDGF-BB by HUVECs

An ELISA assay was used to determine the PDGF-BB concentrations secreted by the HUVECs exposed to 1 Pa or 3 Pa of shear stress and by the control HUVECs exposed to static conditions. ECs exposed to a WSS of 1 Pa secreted more PDGF-BB ($27.93 \pm 5.13 \text{ pg}\cdot\text{ml}^{-1}$) after 4 hours (2 hours of shear stress followed by 2 hours of rest) compared with ECs exposed to a WSS of 3 Pa ($18.50 \pm 7.97 \text{ pg}\cdot\text{ml}^{-1}$) (Fig. 4). Furthermore, ECs in control medium secreted a significant amount of PDGF-BB ($54.93 \pm 15.87 \text{ pg}\cdot\text{ml}^{-1}$) compared with the shear stress-stimulated ECs.

3.2 Model convergence

We applied bootstrap sampling to the $N = 60$ simulations and computed the relative errors (margins between final counts and basal values) on SMCs and

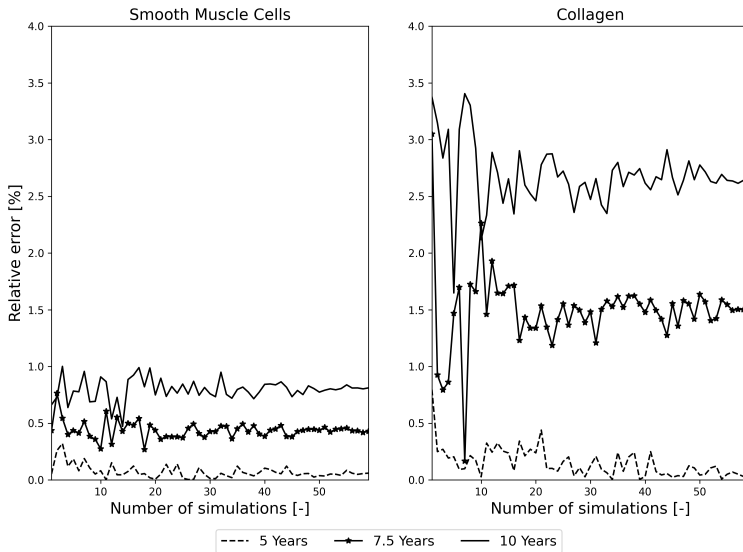


Fig. 5 Relative error of SMCs and Collagen counts as a function of number of simulations and for three different timeframes: 5 years, 7.5 years and 10 years

collagen average counts as a function of the number of simulations. Figure 5 shows that the errors on both averages increased with time. For a timeframe of 10 years, the errors stabilized after $N = 10$ (oscillations $< 1\%$ for Collagen counts) simulations with an average of 0.8% for SMCs and 2.5% for collagen. Therefore, all the results were expressed as the mean (solid lines) of $N=10$ simulations with their 95% confidence interval (shaded region) and normalized to their initial values unless stated otherwise.

3.3 Basal versus vibration exposure states

Figure 6 shows a qualitative representation of both the 'No Vibration' state and the vibration-induced intimal hyperplasia process for different times. The model successfully preserved the baseline geometry of the artery as well as the areas and thicknesses of the layers in the basal state ('No Vibration'). Conversely, during chronic exposure to vibration for 10 years, we observed the formation of a symmetrical intimal hyperplasia characterized by a 42% reduction in the lumen area and an increase of the intimal layer thickness (Fig 7).

In addition, during the 'No Vibration' state, SMCs and collagen normalized counts remained relatively constant. However, they both increased significantly and roughly doubled over 10 years during the vibration exposure state. As for Elastin counts, no significant change was observed between the two simulated conditions (Table 1).

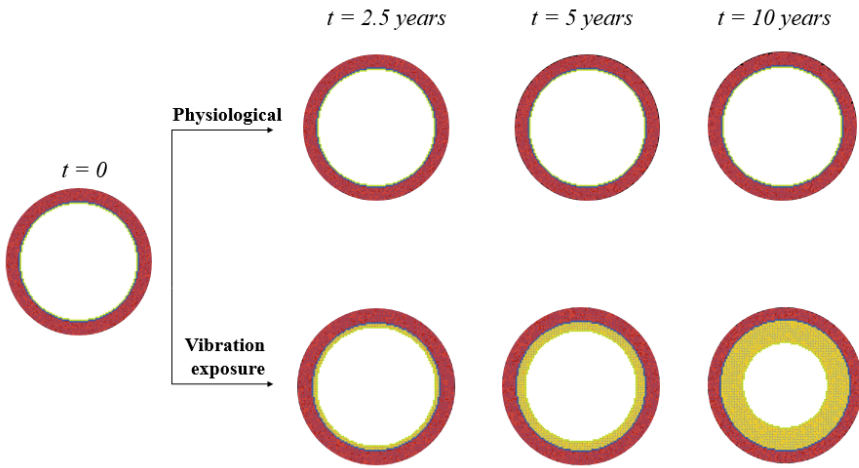


Fig. 6 Qualitative representation of the ABM output of artery geometry during 'No Vibration' and 'Vibration' states

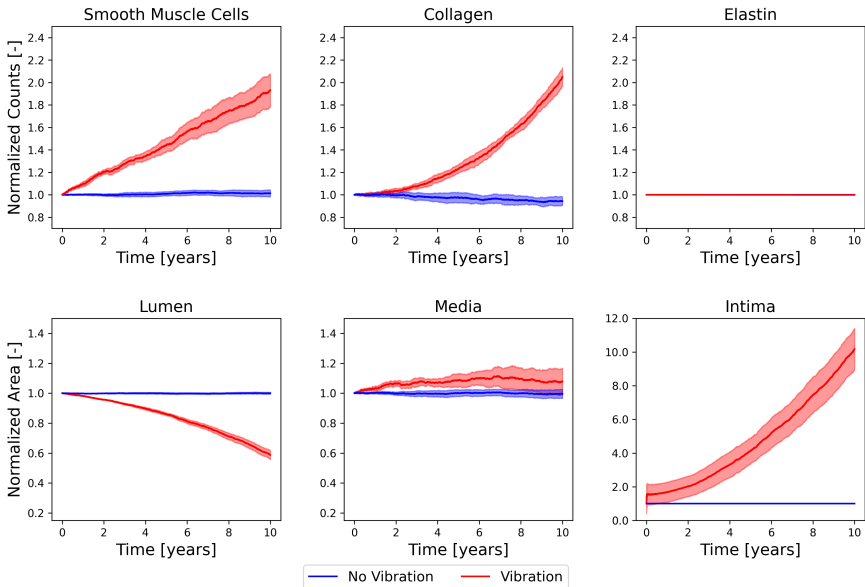


Fig. 7 Evolution of SMCs, Collagen and Elastin counts as well as the lumen, media and intima surfaces during a chronic vibration-induced LSS for a time-frame of $T_{\text{end}} = 10$ years (4 hours of vibration exposure / day). The results are plotted against that of 'No Vibration' state

Table 1 Final outputs of agent counts and layer areas at $t = 10$ years in the 'No Vibration' state and during vibration exposure for 4 hours per day. All the values are normalized to their initial value and are represented as means \pm SD of $N = 10$ simulations.

	No Vibration	Vibration
SMCs counts	1.01 \pm 0.05	1.93 \pm 0.25
Collagen counts	0.94 \pm 0.08	2.05 \pm 0.14
Elastin counts	1.00 \pm 0.00	0.99 \pm 0.002
Lumen area	0.99 \pm 0.01	0.58 \pm 0.05
Media area	0.99 \pm 0.05	1.07 \pm 0.15
Intima area	1.00 \pm 0.00	10.2 \pm 2.14

3.4 Model sensitivity analysis

3.4.1 Influence of WSS-modulated factor secretion by ECs and SMCs

In the absence of TGF- β , SMCs proliferated less compared to the full model and therefore led to less severe formation of stenosis (22% after 10 years instead of 42%) (Fig. 8.A). Moreover, the absence of TGF- β led to a decrease in the media area and less collagen synthesis compared with the full model. On the other hand, the suppression of NO effects on apoptosis did not affect the magnitude of stenosis after 10 years. However, the final SMCs count was lower in the case of NO suppression and thus did not lead to the same increase in media thickness observed in the full model (Fig 8.B). Finally, eliminating the secretion of WSS-regulated MMP-2 had no effects on any of the output values of the model (Fig 8.C)). None of the factors affected the evolution of elastin counts (Fig. 8).

3.4.2 Model sensitivity to the PDGF-BB diffusion coefficient and the diffusion model boundary conditions

When $D_{\text{PDGF-BB}}$ was increased by one order of magnitude, an outward arterial growth was observed characterized by an increase of the media area (Fig. 9). The lumen area decreased slightly after 10 years while the intima slightly thickened with time. Collagen and elastin contents remained unchanged. However, a decrease of $D_{\text{PDGF-BB}}$ triggered an excessive proliferation and migration of SMCs, which in some cases led to the complete occlusion of the artery after 4 years. The media area decreased at first and then started to increase again with time while the intima layer thickened considerably after 4 years. Elastin content was insensitive to the variation of $D_{\text{PDGF-BB}}$.

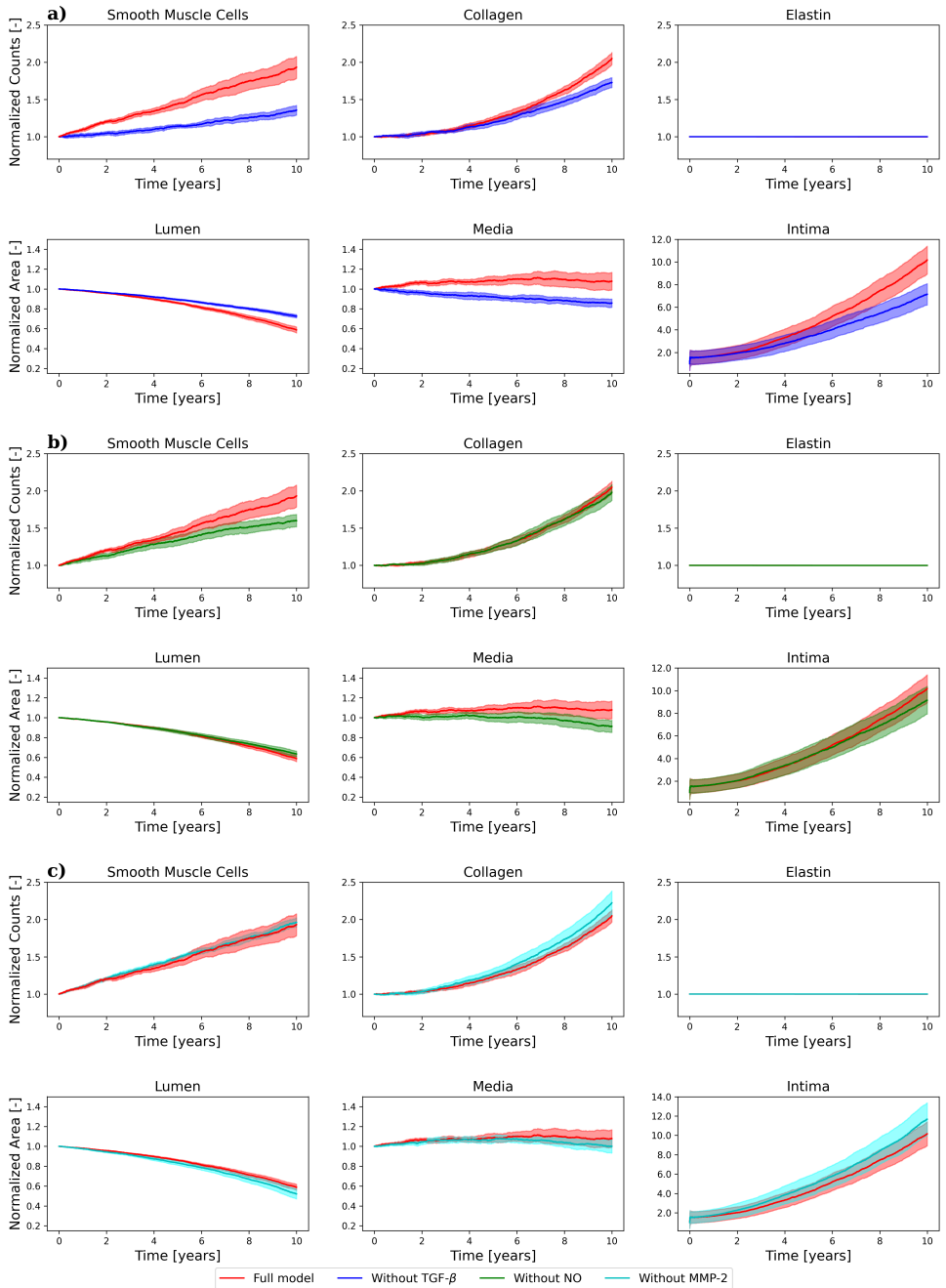


Fig. 8 The influence of: a) EC-secretion of TGF-beta, b) EC-secretion of NO, and c) WSS-modulated SMC-secretion of MMP-2 on the model's behavior. TGF-beta had the most influence on intimal hyperplasia formation while WSS-modulated MMP-2 had no effects on any of the plotted outputs

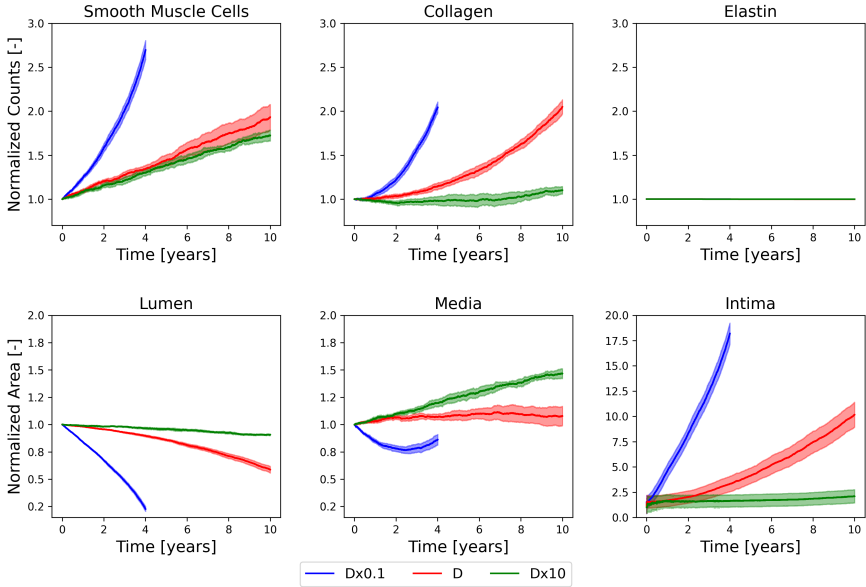


Fig. 9 Sensitivity analysis on $D_{PDGF-BB}$. A decrease of $D_{PDGF-BB}$ by one order of magnitude led to the complete occlusion of the artery in some cases after 4 years of vibration exposure for 4 hours per day while its increase induced the thickening of the media and 10% stenosis after 10 years

Moreover, in the case of infinite boundary conditions, a slight increase of final SMCs counts was observed compared with a closed boundary. Consequently, a thickening of the media area was observed after 5 years. In contrast, the choice of boundary conditions did not affect any of the other agent counts or areas after 5 years (Fig. 10).

3.5 Mechano-regulation of cellular mechanisms

Our model was able to simulate the effects of the vibration-induced WSS values as well as the hoop stress field values on the cellular mechanisms implemented. A decrease in the hoop stress field values inside the arterial wall was observed during arterial growth simulation (Fig. 11). Figure 12 shows the evolution of the output values when the model was stimulated by hemodynamics (τ) and mechanical stresses (σ_θ) simultaneously. The evolution of the total collagen content showed two phases: an initial decrease and then an increase over time. The decrease in collagen was accompanied by a decrease in the media area and a reduction of the lumen reaching 30% after 10 years. Moreover, the mechano-regulation of the cellular mechanisms led to a noticeable degradation of elastin which started to become evident after 5 years. The normalized averages of data are detailed in Table 2.

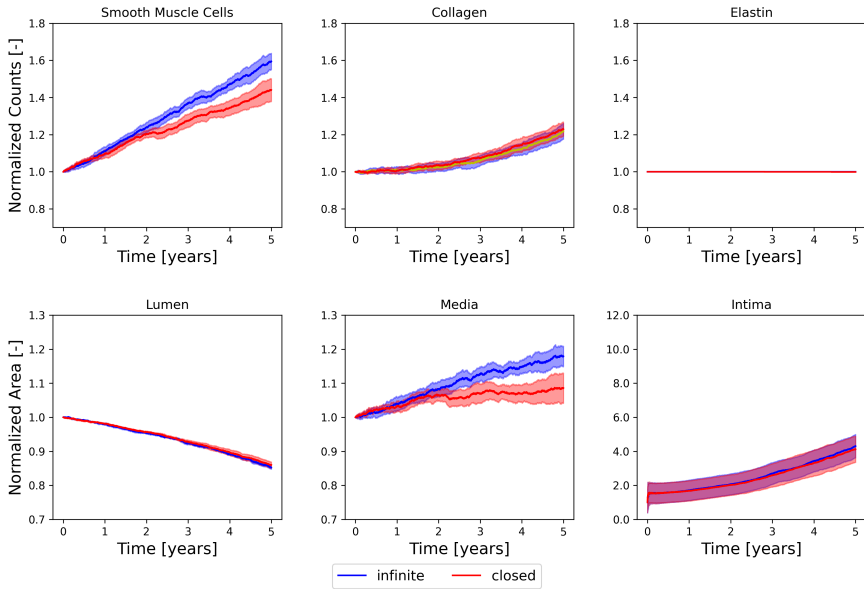


Fig. 10 Effects of the choice of BCs in the GFs diffusion model. The model was run for $T_{\text{end}} = 5$ years. BC choice did not have any effect on the reduction of the lumen area after 5 years

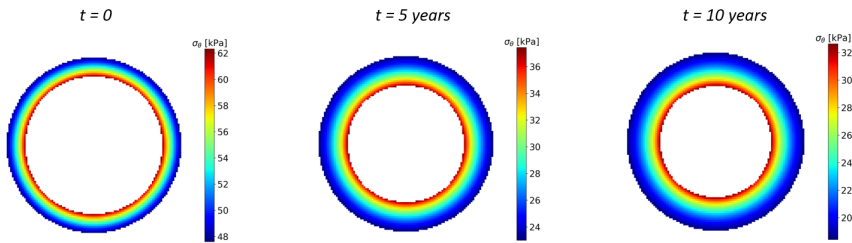


Fig. 11 Evolution of hoop stress values in the arterial wall during time. Values are plotted at $t = 0$ (initial), $t = 5$ years, and $t = 10$ years

4 Discussion

In previous studies, ABMs were used to model vascular adaptation to a mechanical stimulus (Keshavarzian et al, 2018; Thorne et al, 2011; Boyle et al, 2010; Garbey et al, 2015; Zahedmanesh and Lally, 2012; Keshavarzian et al, 2019) or a hemodynamics stimulus (Corti et al, 2020). In many cases, ABMs were coupled with continuum models that provided spatial distributions of circumferential stress or wall shear stress (Corti et al, 2021). These spatial

Table 2 Final outputs of the ABM at $T_{\text{end}} = 10$ years in the case of: i) WSS-only stimulated cellular mechanisms (τ), and ii) WSS-driven and mechanoregulated cellular mechanisms ($\tau + \sigma_{\theta}$).

	τ	$\tau + \sigma_{\theta}$
SMCs counts	1.93 ± 0.25	1.87 ± 0.15
Collagen counts	2.05 ± 0.14	0.80 ± 0.09
Elastin counts	0.99 ± 0.002	0.75 ± 0.04
Lumen area	0.58 ± 0.05	0.70 ± 0.02
Media area	1.07 ± 0.15	0.95 ± 0.10
Intima area	10.2 ± 2.14	7.41 ± 1.48

distributions of mechanical stresses were communicated to the ABMs and regulated the modeled cellular mechanisms, such as SMC proliferation/apoptosis and ECM synthesis/degradation (Corti et al, 2020; Keshavarzian et al, 2018; Zahedmanesh and Lally, 2012). In these studies, cellular mechanisms such as proliferation or migration were modeled as being regulated directly by the mechanical stimulus values without taking into account the secretion of mitogenic and chemotactic factors (Corti et al, 2020; Garbey et al, 2015; Boyle et al, 2010). Consequently, few ABMs captured the hemodynamics-driven and mechanical stress-driven secretion of factors which, after their diffusion inside the artery layers, would modulate cell dynamics (Bhui and Hayenga, 2017; Keshavarzian et al, 2018). In addition, to the best of our knowledge, none of the existing ABMs modeled the effects of the decrease in circumferential stress during hemodynamics-driven arterial growth.

We presented herein an ABM of hemodynamics-driven vibration-induced intimal hyperplasia where we added to the existing frameworks (Garbey et al, 2017; Boyle et al, 2010) by: i) including more relevant soluble factors and studying their effects on cell dynamics, such as the mitogenic effects of TGF- β and the migratory effects of PDGF-BB on SMCs, ii) combining the ABM with experimental results in order to identify the behavioral rules parameters, iii) allowing the mechanoregulation of the cellular mechanisms resulting from the variation of the hoop stress field values during inward arterial growth (increase in the intima layer thickness), and iv) studying the effects of each WSS-modulated biological phenomenon on the model's behavior.

4.1 Combining ABM with experimental tests

First, we considered the secretion of three main factors that regulated SMC proliferation/apoptosis (PDGF-BB, TGF- β and NO) and migration (PDGF-BB) dynamics. PDGF-BB was the crucial factor in our ABM. In addition to its proliferative effects, PDGF-BB is also a chemotactic agent that activates

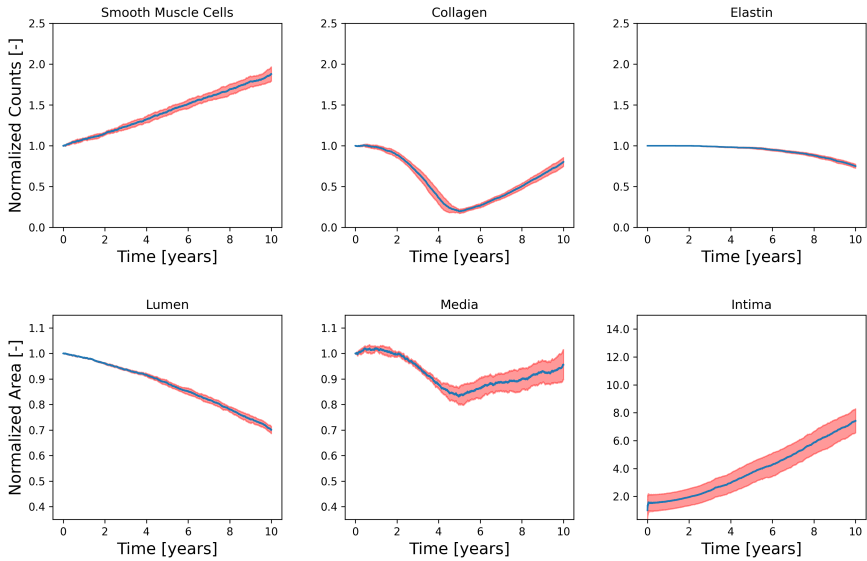


Fig. 12 Evolution of SMCs, Collagen and Elastin counts as well as the lumen, media and intima surfaces during a chronic vibration-induced LSS and including mechanoregulated cellular mechanisms for a timeframe of $T_{\text{end}} = 10$ years. Collagen and Elastin contents of the artery were massively affected by the decrease of σ_{θ} values due to the intimal hyperplasia formation

the migration of SMCs from the media to the intima, which is a key phenomenon in the intimal hyperplasia process. Therefore, the parametrization of the PDGF-BB EC-secretion rule was a key step in our modeling scheme. Most ABMs are dependent on empirical behavior rules that require parametrization to fit biological data. In some studies, a heuristic approach was used to identify the equations parameters by conducting a cycle of calibration and verification by comparing the outputs with histological features (Corti et al, 2020). Other authors obtained their parameters from experimental data found in the literature (Keshavarzian et al, 2018; Thorne et al, 2011; Martin et al, 2015). Our approach consisted in combining experimental tests with our ABM in order to calibrate the ABM parameters according to the experimental in-vitro findings (Thorne et al, 2007). We conducted flow loop experiments on HUVECs to identify the parameters of the law that yields the mass of PDGF-BB secreted by the ECs as a function of WSS (Table A1). Our experimental results showed a similar ratio of PDGF-BB levels between 1 and 3 Pa when compared with literature data (Hsieh et al, 1991). This approach increased confidence in our ABM and helped in calibrating the other parameters derived from the literature for our experimental findings (Thorne et al, 2007).

In our ABM, SMC and ECM dynamics are based on stochastic rules which means that each model run will produce different output values. Therefore, we applied bootstrap sampling to $N = 60$ simulations in basal state to evaluate the evolution of SMC and collagen counts as a function of the number of simulations. We found that after $N = 10$ simulations, the counts stabilized around an average value. This method, similar to that used in (Garbey et al, 2015) helped in identifying the minimum number of simulations needed to obtain an accurate estimation of the output value and to ensure a reasonable computational cost. In addition, we observed that the margin between the final SMCs or collagen counts and their basal counts increased with the increase of the simulation timeframe which means that more simulations are needed when simulating longer timeframes.

4.2 Model's sensitivity to WSS-modulated factors

We studied the impact of all WSS-modulated factors, except the PDGF-BB (the necessary key factor), on the formation of intimal hyperplasia. Among the three factors tested i.e., TGF- β , NO and MMP-2, TGF- β had the most statistically significant effects on SMCs proliferation, media thickness and intimal hyperplasia formation (Online Resources Figure S2 and Table S1). Furthermore, NO effects were clearly visible on SMC proliferation in the media whereas the lumen and the intima surfaces were not statistically different ($p > 0.05$) from those of the full model (Online Resources Figure S2 and Table S1). This demonstrates that the magnitude of stenosis during intimal hyperplasia depends on the PDGF-BB-induced SMC migration as well as on the proliferative effects TGF- β and PDGF-BB on the SMCs inside the intima.

Our results showed that WSS-modulated MMP-2 had no statistically significant effects on any of the model outputs (Online Resources Table S1). MMP-2 is an enzyme that, when present in the media, is responsible for collagen and elastin degradation (Sakamoto et al, 2006; Garanich et al, 2005). Consequently, in the case of MMP-2 suppression we should expect a final count of collagen in the media higher than that of the full model. However, the collagen and elastin degradation rates between the full model and the model without MMP-2 were not significantly different (Online Resources Table S1 and Figure S2). This demonstrates that the levels of WSS-modulated MMP-2 did not induce a degradation rate that would lead to a loss of ECM agents. Indeed, ECM agents were assigned collagen or elastin masses equal to 0.84 ng. When a degradation event was performed (Table A4), one ECM agent corresponding to either collagen or elastin was removed from the ABM. Thus, the elastin and collagen degradation in our model would only be visible if the MMP-2 quantities degraded a collagen or elastin mass equivalent to 0.84 ng. Hence, any variation of ECM mass less than the mass of one agent would not be visible in our model.

4.3 Model's sensitivity to PDGF-BB diffusion coefficient

The sensitivity analysis on the $D_{\text{PDGF-BB}}$ coefficient showed that a decrease by one order of magnitude would lead to complete stenosis after 4 years. However, by increasing the $D_{\text{PDGF-BB}}$ value, the model would tend to an outward growth characterized by an increase of the media area with a slightly decreased lumen area. Indeed, a higher diffusion coefficient yielded a lower local mass of PDGF-BB around SMCs, bringing about a decrease of PDGF-BB-induced migration and SMC proliferation rates. Our results show that this decrease in diffused PDGF-BB mass had a minor effect on SMC counts while an increase of media thickness was observed. Indeed, with a lower PDGF-BB mass, fewer SMCs would migrate from the media to the intima while still undergoing proliferation owing to other factors (TGF- β and NO), which would lead to an increase in media thickness. Additionally, only a slight decrease of the lumen area was observed. This indicates that a few SMCs migrated from the media to the intima, thus highlighting that the effects of PDGF-BB on the chemotactic migration of SMCs were crucial to the intimal hyperplasia process. These results are consistent with the study of [Jawien et al \(1992\)](#) which found that migration accounts for most PDGF-BB effects on SMCs and that intimal thickening depends mostly on SMCs migration from the media to the intima. In addition, the resulting PDGF-BB concentration had an effect on the proliferation/migration ratio. In addition, our model is capable of differentiating between outward and inward growth depending on the ratio between SMC migration and the proliferation rates dictated by the PDGF-BB concentration resulting from the diffusion model.

4.4 Atrophic response to the fall in hoop stress

When the hoop stress effects were added to the model, the collagen and elastin contents of the media were significantly affected by the mechanoregulated MMP-2. As can be seen in Online Resources Fig.S.4, the collagen in the media was fully degraded after 5 years and the elastin content fell by 25% after 10 years. Our model was able to capture the upregulation of MMP-2 and the degradation of ECM in the case of a fall in circumferential stress in the arterial wall. The mechanoregulated degradation of collagen in the media was greater than the SMC proliferation resulting from the vibration-induced LSS, leading to a subsequent decrease of media thickness until all the collagen was degraded ([Fig. 12](#)). These results are consistent with the findings of [Bayer et al \(1999\)](#) on the atrophic response of a cuffed artery. These authors observed a decrease in collagen content and a reduction of the media thickness due to the decrease in circumferential stress stemming from lowering arterial wall tension. However, we did not observe a decay of SMCs in the media, as suggested by the experimental findings. This was due to the application of a chronic vibration-induced LSS that induced SMC proliferation; these mechanisms were not taken into account in the study of [Bayer et al \(1999\)](#). In our model, the atrophic response to the fall in circumferential stress was manifested as less severe intima growth

in the case of mechanoregulated versus WSS-only regulated cellular mechanisms. In addition, our model predicted that the ECM content in the media was mainly regulated by the circumferential stress field ([Keshavarzian et al, 2018](#)).

4.5 Limitations

Although our model was able to capture the vibration-induced intimal hyperplasia process, it was built on important assumptions and ignored many aspects that could have affected the final output of the model. First, the WSS values applied to the endothelium to match the presence or absence of vibrations were imposed as two constant values and were not retrieved from a computational fluid dynamics model (CFD). Secondly, the model was built using a 2D symmetrical circular geometry of the artery. The agents movements inside the ABMs and the regularization algorithms were limited to a 2D representation. However, in reality, the SMCs would have more possibilities for movement which would likely affect arterial growth over time. In future work, our ABM will be coupled with a CFD model of a reconstructed 3D geometry of a digital artery to provide a more accurate profile of WSS values ([Corti et al, 2020](#)). Our ABM equations were built using experimental data obtained from vascular cells in-vitro. However, most of the experimental data were derived from short term tests and applied in long term simulations in our model. Thus, long term behaviors of the artery were ignored during the 10-year timeframe of the simulation in which the parameters of the cellular mechanisms modeled remained unchanged. Additionally, we modeled the effects of five factors that affected the SMC (PDGF-BB, TGF- β and NO) and ECM (MMP-2 and MMP-9) dynamics. The choice of these factors was based on an extensive literature review on hemodynamics effects on vascular cells. Our goal was to identify the most relevant factors involved in intimal hyperplasia. However, during this process, other hemodynamics-driven cellular mechanisms were ignored such as the effects of PDGF-AA and PDGF-AB on SMC proliferation and migration ([Li et al, 2011](#)). Including natural ageing mechanisms in the artery behavior and incorporating other hemodynamic-driven factors could be considered to improve the model.

In order to identify the mathematical formulations and the associated parameters of each behavior rule, we applied an empirical approach to fit experimental data to numerical models and we chose the model with the best fit. However, in some cases, experimental data was scarce and the numerical models were built with few fitting points (Appendix A). In our framework, we combined experimental tests with our ABM to identify the parameters of the PDGF-BB secretion rule. However, we tested only two WSS values and still needed literature data to build the equations. Moreover, the lack of histological data demonstrating the time course of the stenosis formation with workers exposed to HAVs In future work, more experimental investigations will be conducted for each cellular mechanism implemented associated with a validation process at each step between numerical and experimental outcomes

to ensure more accurate calibration of the parameters. Unfortunately, due to a lack of data demonstrating the time course of vibration-induced stenosis in workers exposed to HAVs, the validation step of our model's outputs was not conducted in this study. Nonetheless, ex-vivo experiments that investigate the effects of WSS on digital arteries will be considered in future works and will allow the validation of our model (Noël et al, 2022).

Finally, one of the main drawbacks of our ABM was the long computational time of one simulation (≥ 24 hours). In order to minimize the computational cost, our code was optimized using parallelization when possible and a speed analysis was conducted on each part of the code. Our analysis showed that the computational load relied mainly in the communication routines between Python and NetLogo. Therefore, one of the solutions considered would be to transition to a Python only code which would decrease the computational cost and limit the need to one computational environment only.

We presented herein an ABM of vibration-induced intimal hyperplasia. The main finding of the study was the model's ability to predict 30% stenosis after 10 years of vibration exposure for 4 hours a day. Our sensitivity analysis showed that TGF- β was the most relevant WSS-modulated factor alongside PDGF-BB that contributed the most to intimal hyperplasia formation. Further experimental investigations on the EC-secretion of TGF- β and the diffusion coefficient of factors could be planned to recalibrate the related parameters. We also showed that the decrease of circumferential stress plays a major role in ECM regulation inside the media and cannot be ignored when modelling the intimal hyperplasia process. To this end, our ABM will be coupled with an anisotropic hyperelastic mechanical model that will provide a better estimation of circumferential stress. In addition, by using a mechanical model that takes into account the change in mechanical stiffness as a response to arterial remodeling, which may affect the factors secretion by the vascular cells, will allow our model to make more accurate predictions. In terms of safety and the prevention of occupational accidents, the model's predictions will be compared to the progression of stenosis in workers exposed to HAVs in order to prevent the onset of the vibration-induced Raynaud's syndrome.

Supplementary information. The online version of this article contains supplementary material.

Acknowledgements.

Declarations

- **Funding** The authors did not receive support from any organization for the work submitted.
- **Financial interests** All the authors certify that they have no affiliations with or involvement in any organization or entity with any financial interest or non-financial interest in the subject matter or materials discussed in this manuscript.
- **Ethics approval** Not applicable

- **Consent to participate** Not applicable
- **Consent for publication** Not applicable
- **Availability of data and materials** Not applicable
- **Code availability** Not applicable
- **Authors' contributions** Conceptualization: M.R. and C.N. and E.J.; Formal Analysis: M.R. and C.N.; Funding acquisition: C.N.; Investigation: M.R. and C.N. Methodology: M.R. and C.N. and N.S. and J.C. and A.L. and G.R. (section 2.3) and E.J.; Project administration: C.N.; Resources: C.N.; Software: M.R.; Supervision: C.N. and E.J.; Validation: C.N. and N.S. and J.C. and E.J.; Visualization: M.R.; Writing - original draft preparation: M.R.; Writing - review and editing: C.N. and N.S. and J.C. and A.L. and E.J.

References

- Albro MB, Nims RJ, Cigan AD, et al (2013) Accumulation of exogenous activated TGF- β in the superficial zone of articular cartilage. *Biophysical Journal* 104(8):1794–1804. <https://doi.org/10.1016/j.bpj.2013.02.052>
- Andrews AM, Jaron D, Buerk DG, et al (2010) Direct, real-time measurement of shear stress-induced nitric oxide produced from endothelial cells in vitro. *Nitric Oxide* 23(4):335–342. <https://doi.org/10.1016/j.niox.2010.08.003>
- Ashe WF, Williams N (1964) Occupational Raynaud's II: Further studies of this disorder in uranium mine workers. *Archives of Environmental Health: An International Journal* 9(4):425–433. <https://doi.org/10.1080/00039896.1964.10663861>
- Bayer IM, Adamson SL, Langille BL (1999) Atrophic remodeling of the artery-cuffed artery. *Arteriosclerosis, Thrombosis, and Vascular Biology* 19(6):1499–1505. <https://doi.org/10.1161/01.ATV.19.6.1499>
- Bhui R, Hayenga HN (2017) An agent-based model of leukocyte transendothelial migration during atherogenesis. *PLoS Computational Biology* 13(5):e1005523. <https://doi.org/10.1371/journal.pcbi.1005523>
- Bornfeldt KE, Raines EW, Nakano T, et al (1994) Insulin-like growth factor-I and platelet-derived growth factor-BB induce directed migration of human arterial smooth muscle cells via signaling pathways that are distinct from those of proliferation. *Journal of Clinical Investigation* 93(3):1266–1274. <https://doi.org/10.1172/JCI117081>
- Bovenzi M, Griffin MJ (1997) Haemodynamic changes in ipsilateral and contralateral fingers caused by acute exposures to hand transmitted vibration. *Occupational and Environmental Medicine* 54(8):566–576. <https://doi.org/10.1136/oem.54.8.566>

- Bovenzi M, Giansante C, Fiorito A, et al (1985) Relation of haemostatic function, neurovascular impairment, and vibration exposure in workers with different stages of vibration induced white finger. *British Journal of Industrial Medicine* 42(4):253–259. <https://doi.org/10.1136/oem.42.4.253>
- Boyle CJ, Lennon AB, Early M, et al (2010) Computational simulation methodologies for mechanobiological modelling: A cell-centred approach to neointima development in stents. *Philosophical Transactions of the Royal Society A: Mathematical, Physical and Engineering Sciences* 368(1921):2919–2935. <https://doi.org/10.1098/rsta.2010.0071>
- Brammer AJ, Pitts PM (2012) Frequency weighting for vibration-induced white finger compatible with exposure-response models. *Industrial Health* 50(5):397–411. <https://doi.org/10.2486/indhealth.MS1383>
- Brammer AJ, Taylor W, Lundborg G (1987) Sensorineural stages of the hand-arm vibration syndrome. *Scandinavian Journal of Work, Environment and Health* 13(4):279–283. <https://doi.org/10.5271/sjweh.2050>
- Chapman GB, Durante W, Hellums JD, et al (2000) Physiological cyclic stretch causes cell cycle arrest in cultured vascular smooth muscle cells. *American Journal of Physiology-Heart and Circulatory Physiology* 278(3):748–754. <https://doi.org/10.1152/ajpheart.2000.278.3.H748>
- Cóndor M, Rüberg T, Borau C, et al (2018) A web-based application for automated quantification of chemical gradients induced in microfluidic devices. *Computers in Biology and Medicine* 95:118–128. <https://doi.org/10.1016/j.combiomed.2018.02.001>
- Corti A, Chiastra C, Colombo M, et al (2020) A fully coupled computational fluid dynamics – agent-based model of atherosclerotic plaque development: Multiscale modeling framework and parameter sensitivity analysis. *Computers in Biology and Medicine* 118:103623. <https://doi.org/10.1016/j.combiomed.2020.103623>
- Corti A, Colombo M, Migliavacca F, et al (2021) Multiscale computational modeling of vascular adaptation: a systems biology approach using agent-based models. *Frontiers in Bioengineering and Biotechnology* 9:744560. <https://doi.org/10.3389/fbioe.2021.744560>
- Cucina A, Sterpetti AV, Borrelli V, et al (1998) Shear stress induces transforming growth factor- β 1 release by arterial endothelial cells. *Surgery* 123(2):212–217. [https://doi.org/10.1016/S0039-6060\(98\)70260-0](https://doi.org/10.1016/S0039-6060(98)70260-0)
- Curry BD, Bain JL, Yan JG, et al (2002) Vibration injury damages arterial endothelial cells. *Muscle and Nerve* 25(4):527–534. <https://doi.org/10.1002/mus.10058>

- Dardik A, Yamashita A, Aziz F, et al (2005) Shear stress-stimulated endothelial cells induce smooth muscle cell chemotaxis via platelet-derived growth factor-BB and interleukin-1 α . *Journal of Vascular Surgery* 41(2):321–331. <https://doi.org/10.1016/j.jvs.2004.11.016>
- DiMilla PA, Stone JA, Quinn JA, et al (1993) Maximal migration of human smooth muscle cells on fibronectin and type IV collagen occurs at an intermediate attachment strength. *Journal of Cell Biology* 122(3):729–737. <https://doi.org/10.1083/jcb.122.3.729>
- Donadoni F, Pichardo-Almarza C, Bartlett M, et al (2017) Patient-specific, multi-scale modeling of neointimal hyperplasia in vein grafts. *Frontiers in Physiology* 8:226. <https://doi.org/10.3389/fphys.2017.00226>
- Donati P, Schust M, Szopa J, et al (2008) Workplace exposure to vibration in Europe: an expert review. European Agency for Safety and Health at Work, European risk observatory report
- EN NF ISO 5349-1:2001 (2002) Mechanical vibration – Measurement and evaluation of human exposure to hand-transmitted vibration – Part 1: General requirements. AFNOR, Paris
- Epstein FH, Gibbons GH, Dzau VJ (1994) The emerging concept of vascular remodeling. *New England Journal of Medicine* 330(20):1431–1438. <https://doi.org/10.1056/NEJM199405193302008>
- Evans DJ, Lawford PV, Gunn J, et al (2008) The application of multiscale modelling to the process of development and prevention of stenosis in a stented coronary artery. *Philosophical Transactions of the Royal Society A: Mathematical, Physical and Engineering Sciences* 366(1879):3343–3360. <https://doi.org/10.1098/rsta.2008.0081>
- Fischer GM, Llaurado JG (1966) Collagen and elastin content in canine arteries selected from functionally different vascular beds. *Circulation research* 19(2):394–399. <https://doi.org/10.1161/01.RES.19.2.394>
- Garanich JS, Pahakis M, Tarbell JM (2005) Shear stress inhibits smooth muscle cell migration via nitric oxide-mediated downregulation of matrix metalloproteinase-2 activity. *American Journal of Physiology-Heart and Circulatory Physiology* 288(5):H2244–H2252. <https://doi.org/10.1152/ajpheart.00428.2003>
- Garbey M, Rahman M, Berceci S (2015) A multiscale computational framework to understand vascular adaptation. *Journal of Computational Science* 8:32–47. <https://doi.org/10.1016/j.jocs.2015.02.002>

- Garbey M, Casarin S, Berceci SA (2017) Vascular adaptation: pattern formation and cross validation between an agent based model and a dynamical system. *Journal of Theoretical Biology* 429:149–163. <https://doi.org/10.1016/j.jtbi.2017.06.013>
- Gay CG, Winkles JA (1991) The half-lives of platelet-derived growth factor A- and B-chain mRNAs are similar in endothelial cells and unaffected by heparin-binding growth factor-1 or cycloheximide. *Journal of Cellular Physiology* 147(1):121–127. <https://doi.org/10.1002/jcp.1041470116>
- Gerthoffer WT (2007) Mechanisms of vascular smooth muscle cell migration. *Circulation Research* 100(5):607–621. <https://doi.org/10.1161/01.RES.0000258492.96097.47>
- Gleason RL, Humphrey JD (2004) A mixture model of arterial growth and remodeling in hypertension: Altered muscle tone and tissue turnover. *Journal of Vascular Research* 41(4):352–363. <https://doi.org/10.1159/000080699>
- Heydarkhan-Hagvall S, Chien S, Nelander S, et al (2006) DNA microarray study on gene expression profiles in co-cultured endothelial and smooth muscle cells in response to 4- and 24-h shear stress. *Molecular and Cellular Biochemistry* 281(1-2):1–15. <https://doi.org/10.1007/s11010-006-0168-6>
- Holzapfel GA, Gasser TC, Ogden RW (2000) A new constitutive framework for arterial wall mechanics and a comparative study of material models. *Journal of Elasticity* 61:1–48. <https://doi.org/10.1023/A:1010835316564>
- Horvat N, Virag L, Holzapfel GA, et al (2019) A finite element implementation of a growth and remodeling model for soft biological tissues: Verification and application to abdominal aortic aneurysms. *Computer Methods in Applied Mechanics and Engineering* 352:586–605. <https://doi.org/10.1016/j.cma.2019.04.041>
- Hsieh HJ, Li NQ, Frangos JA (1991) Shear stress increases endothelial platelet-derived growth factor mRNA levels. *American Journal of Physiology-Heart and Circulatory Physiology* 260(2):H642–H646. <https://doi.org/10.1152/ajpheart.1991.260.2.H642>
- Humphrey JD, Rajagopal KR (2002) A constrained mixture model for growth and remodeling of soft tissues. *Mathematical Models and Methods in Applied Sciences* 12(3):407–430. <https://doi.org/10.1142/S0218202502001714>
- Isenberg BC, DiMilla PA, Walker M, et al (2009) Vascular smooth muscle cell durotaxis depends on substrate stiffness gradient strength. *Biophysical Journal* 97(5):1313–1322. <https://doi.org/10.1016/j.bpj.2009.06.021>

- Jawien A, Bowen-Pope DF, Lindner V, et al (1992) Platelet-derived growth factor promotes smooth muscle migration and intimal thickening in a rat model of balloon angioplasty. *The Journal of Clinical Investigation* 99(2):507–511. <https://doi.org/10.1172/JCI115613>
- Jaxa-Rozen M, Kwakkel JH (2018) PyNetLogo: Linking NetLogo with Python. *Journal of Artificial Societies and Social Simulation* 21(2):4. <https://doi.org/10.18564/jasss.3668>
- Kanai AJ, Strauss HC, Truskey GA, et al (1995) Shear stress induces ATP-independent transient nitric oxide release from vascular endothelial cells, measured directly with a porphyrinic microsensor. *Circulation Research* 77(2):284–293. <https://doi.org/10.1161/01.RES.77.2.284>
- Keshavarzian M, Meyer CA, Hayenga HN (2018) Mechanobiological model of arterial growth and remodeling. *Biomechanics and Modeling in Mechanobiology* 17(1):87–101. <https://doi.org/10.1007/s10237-017-0946-y>
- Keshavarzian M, Meyer CA, Hayenga HN (2019) In silico tissue engineering: a coupled agent-based finite element approach. *Tissue Engineering Part C: Methods* 25(11):641–654. <https://doi.org/10.1089/ten.tec.2019.0103>
- Kona S, Chellamuthu P, Xu H, et al (2009) Effects of cyclic strain and growth factors on vascular smooth muscle cell responses. *The Open Biomedical Engineering Journal* 3(1):28–38. <https://doi.org/10.2174/1874120700903010028>
- Koyama N, Hart CE, Clowes AW (1994) Different functions of the platelet-derived growth factor- α and - β receptors for the migration and proliferation of cultured baboon smooth muscle cells. *Circulation Research* 75(4):682–691. <https://doi.org/10.1161/01.RES.75.4.682>
- Krick S, Platoshyn O, Sweeney M, et al (2002) Nitric oxide induces apoptosis by activating K⁺ channels in pulmonary vascular smooth muscle cells. *American Journal of Physiology-Heart and Circulatory Physiology* 282(1):H184–H193. <https://doi.org/10.1152/ajpheart.2002.282.1.H184>
- Kuhl E, Maas R, Himpel G, et al (2007) Computational modeling of arterial wall growth. *Biomechanics and Modeling in Mechanobiology* 6(5):321–331. <https://doi.org/10.1007/s10237-006-0062-x>
- Li L, Blumenthal DK, Terry CM, et al (2011) PDGF-induced proliferation in human arterial and venous smooth muscle cells: Molecular basis for differential effects of PDGF isoforms. *Journal of Cellular Biochemistry* 112(1):289–298. <https://doi.org/10.1002/jcb.22924>

- Martin KS, Blemker SS, Peirce SM (2015) Agent-based computational model investigates muscle-specific responses to disuse-induced atrophy. *Journal of Applied Physiology* 118(10):1299–1309. <https://doi.org/10.1152/jappphysiol.01150.2014>
- Menzel A (2007) A fibre reorientation model for orthotropic multiplicative growth. *Biomechanics and Modeling in Mechanobiology* 6(5):303–320. <https://doi.org/10.1007/s10237-006-0061-y>
- Minion DJ, Snajdar RM, van de Kerkhove MP, et al (2000) The migratory response to platelet-derived growth factor of smooth muscle cells isolated from synthetic vascular grafts in a canine model. *Journal of Vascular Surgery* 31(5):953–959. <https://doi.org/10.1067/mva.2000.106419>
- Nerem RM, Alexander RW, Chappell DC, et al (1998) The study of the influence of flow on vascular endothelial biology. *The American Journal of the Medical Sciences* 316(3):169–175. URL <https://www.sciencedirect.com/science/article/abs/pii/S0002962915403970>
- Newby AC, Zaltsman AB (2000) Molecular mechanisms in intimal hyperplasia. *Journal of Pathology* 190(3):300–309. [https://doi.org/10.1002/\(SICI\)1096-9896\(200002\)190:3<300::AID-PATH596>3.0.CO;2-I](https://doi.org/10.1002/(SICI)1096-9896(200002)190:3<300::AID-PATH596>3.0.CO;2-I)
- Nishio E, Fukushima K, Shiozaki M, et al (1996) Nitric oxide donor SNAP induces apoptosis in smooth muscle cells through cGMP-independent mechanism. *Biochemical And Biophysical Research Communications* 221(1):163–168. <https://doi.org/https://doi.org/10.1006/bbrc.1996.0563>
- Noël C, Settembre N (2022) Assessing mechanical vibration-altered wall shear stress in digital arteries. *Journal of Biomechanics* 131:110893. <https://doi.org/10.1016/j.jbiomech.2021.110893>
- Noël C, Settembre N, Reda M, et al (2022) A multiscale approach for predicting certain effects of hand-transmitted vibration on finger arteries. *Vibration* 5(2):213–237. <https://doi.org/10.3390/vibration5020014>
- Ohno M, Cooke JP, Dzau VJ, et al (1995) Fluid shear stress induces endothelial transforming growth factor beta-1 transcription and production. Modulation by potassium channel blockade. *Journal of Clinical Investigation* 95(3):1363–1369. <https://doi.org/10.1172/JCI117787>
- Okada A, Inaba R, Furuno T (1987) Occurrence of intimal thickening of the peripheral arteries in response to local vibration. *British Journal of Industrial Medicine* 44(7):470–475. <https://doi.org/10.1136/oem.44.7.470>

- Palumbo R, Gaetano C, Antonini A, et al (2002) Different effects of high and low shear stress on platelet-derived growth factor isoform release by endothelial cells: Consequences for smooth muscle cell migration. *Arteriosclerosis, Thrombosis, and Vascular Biology* 22(3):405–411. <https://doi.org/10.1161/hq0302.104528>
- Rodriguez EK, Hoger A, McCulloch AD (1994) Stress-dependent finite growth in soft elastic tissues. *Journal of Biomechanics* 27(4):455–467. [https://doi.org/10.1016/0021-9290\(94\)90021-3](https://doi.org/10.1016/0021-9290(94)90021-3)
- Rouillard AD, Holmes JW (2014) Coupled agent-based and finite-element models for predicting scar structure following myocardial infarction. *Progress in Biophysics and Molecular Biology* 115(2-3):235–243. <https://doi.org/10.1016/j.pbiomolbio.2014.06.010>
- Sakamoto N, Ohashi T, Sato M (2006) Effect of fluid shear stress on migration of vascular smooth muscle cells in cocultured model. *Annals of Biomedical Engineering* 34(3):408–415. <https://doi.org/10.1007/s10439-005-9043-y>
- Sjölund M, Madsen K, von der Mark K, et al (1986) Phenotype modulation in primary cultures of smooth-muscle cells from rat aorta: Synthesis of collagen and elastin. *Differentiation* 32(2):173–180. <https://doi.org/10.1111/j.1432-0436.1986.tb00570.x>
- Sjölund M, Hedin U, Sejersen T, et al (1988) Arterial smooth muscle cells express platelet-derived growth factor (PDGF) A chain mRNA, secrete a PDGF-like mitogen, and bind exogenous PDGF in a phenotype- and growth state-dependent manner. *The Journal of Cell Biology* 106(2):403–413. <https://doi.org/10.1083/jcb.106.2.403>
- Takeuchi T, Futatsuka M, Imanishi H, et al (1986) Pathological changes observed in the finger biopsy of patients with vibration-induced white finger. *Scandinavian Journal of Work, Environment and Health* 12(4):280–283. URL <http://www.jstor.org/stable/40965348>
- Thorne BC, Bailey AM, Peirce SM (2007) Combining experiments with multi-cell agent-based modeling to study biological tissue patterning. *Briefing in Bioinformatics* 8(4):245–257. <https://doi.org/10.1093/bib/bbm024>
- Thorne BC, Hayenga HN, Humphrey JD, et al (2011) Toward a multi-scale computational model of arterial adaptation in hypertension: verification of a multi-cell agent-based model. *Frontiers in Physiology* 2:20. <https://doi.org/10.3389/fphys.2011.00020>
- Todd ME, Laye CG, Osborne DN (1983) The dimensional characteristics of smooth muscle in rat blood vessels. A computer-assisted analysis. *Circulation Research* 53(3):319–331. <https://doi.org/10.1161/01.RES.53.3.319>

- Wakefield LM, Winokur TS, Hollands RS, et al (1990) Recombinant latent transforming growth factor beta 1 has a longer plasma half-life in rats than active transforming growth factor beta 1, and a different tissue distribution. *The Journal of Clinical Investigation* 86(6):1976–1984. <https://doi.org/10.1172/JCI114932>
- Watson MG, Byrne HM, Macaskill C, et al (2020) A multiphase model of growth factor-regulated atherosclerotic cap formation. *Journal of Mathematical Biology* 81(2):725–767. <https://doi.org/10.1007/s00285-020-01526-6>
- Welsh CL (1980) The effect of vibration on digital blood flow. *British Journal of Surgery* 67(10):708–710. <https://doi.org/10.1002/bjs.1800671009>
- Wilensky U (1999) Netlogo. Center for Connected Learning and Computer-Based Modeling, Northwestern University, Evanston, IL URL <http://ccl.northwestern.edu/netlogo/>
- Wolf SC, Sauter G, Rodemann HP, et al (2005) Influence of growth factors on the proliferation of vascular smooth muscle cells isolated from subtotaly nephrectomized rats after endothelin or angiotensin II antagonism. *Nephrology Dialysis Transplantation* 20(2):312–318. <https://doi.org/10.1093/ndt/gfh606>
- Zahedmanesh H, Lally C (2012) A multiscale mechanobiological modelling framework using agent-based models and finite element analysis: application to vascular tissue engineering. *Biomechanics and Modeling in Mechanobiology* 11(3-4):363–377. <https://doi.org/10.1007/s10237-011-0316-0>

Appendix A ABM rules

The biological mechanisms modeled inside the ABM are expressed using mathematical formulations derived from experimental data obtained from our flow loop experiments and from literature data. In all the graphs, the red dots correspond to the experimental data and the solid lines are the fitted models.

Appendix B ABM parameters

Table A1 WSS-dependent factors secretion.

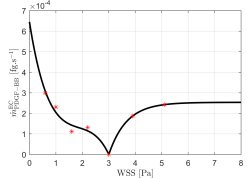
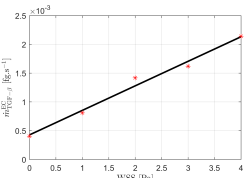
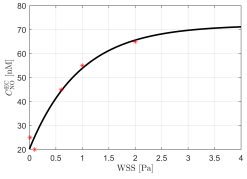
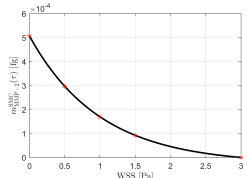
Parameter	Equation	Graphs and References
Mass production rate of PDGF-BB by one EC (EC-secreted) $\dot{m}_{\text{PDGF-BB}}^{\text{EC}}(\tau)$ [$\text{fg}\cdot\text{s}^{-1}$]	$\dot{m}_{\text{PDGF-BB}}^{\text{EC}}(\tau) = \alpha Q_{\text{PDGF-BB}}^1 (1 - \exp(-(\tau - \tau_{\text{phys}})/\kappa_{\text{PDGF-BB}}^1)) + Q_{\text{PDGF-BB}}^2 (1 - \exp((\tau - \tau_{\text{phys}})/\kappa_{\text{PDGF-BB}}^2)) + q_{\text{PDGF-BB}}(\tau - \tau_{\text{phys}})$ $\tau_{\text{phys}} = 3 \text{ Pa}$ <p>if $0.6 \leq \tau \leq 3 \text{ Pa}$:</p> $\alpha = -1,$ $Q_{\text{PDGF-BB}}^1 = 5.44 \times 10^{-5} \text{ fg}\cdot\text{s}^{-1},$ $\kappa_{\text{PDGF-BB}}^1 = 1 \text{ Pa}, Q_{\text{PDGF-BB}}^2 = 5.15 \times 10^{-4} \text{ fg}\cdot\text{s}^{-1},$ $\kappa_{\text{PDGF-BB}}^2 = 1 \text{ Pa},$ $q_{\text{PDGF-BB}} = 2.94 \times 10^{-4} \text{ fg}\cdot\text{s}^{-1}\cdot\text{Pa}^{-1}$ <p>if $\tau \geq 3 \text{ Pa}$:</p> $\alpha = 1,$ $Q_{\text{PDGF-BB}}^1 = 2.54 \times 10^{-4} \text{ fg}\cdot\text{s}^{-1},$ $\kappa_{\text{PDGF-BB}}^1 = 0.6746 \text{ Pa}, Q_{\text{PDGF-BB}}^2 = 0 \text{ fg}\cdot\text{s}^{-1},$ $\kappa_{\text{PDGF-BB}}^2 = 1 \text{ Pa},$ $q_{\text{PDGF-BB}} = 0 \text{ fg}\cdot\text{s}^{-1}\cdot\text{Pa}^{-1}$	 <p>Hsieh et al (1991), Cellular tests</p>
Mass production rate of TGF- β by one EC (EC-secreted) $\dot{m}_{\text{TGF-}\beta}^{\text{EC}}(\tau)$ [$\text{fg}\cdot\text{s}^{-1}$]	$\dot{m}_{\text{TGF-}\beta}^{\text{EC}}(\tau) = Q_{\text{TGF-}\beta} + q_{\text{TGF-}\beta} \times \tau$ $Q_{\text{TGF-}\beta} = 4.26 \times 10^{-4} \text{ fg}\cdot\text{s}^{-1}$ $q_{\text{TGF-}\beta} = 4.26 \times 10^{-4} \text{ fg}\cdot\text{s}^{-1}\cdot\text{Pa}^{-1}$	 <p>Ohno et al (1995), Cucina et al (1998)</p>
NO molar concentration (EC-secreted) $C_{\text{NO}}^{\text{EC}}(\tau)$ [nM]	$C_{\text{NO}}^{\text{EC}}(\tau) = C_1 (1 - \exp(-\tau/\kappa_{\text{NO}})) + C_2$ $C_1 = 51.7 \times T \text{ [nM]}, \kappa_{\text{NO}} = 0.95 \text{ Pa}$ $C_2 = 20.22 \times T \text{ [nM]}$ $T \text{ [hours]}$	 <p>Andrews et al (2010)</p>
Mass of MMP-2 by one SMC $m_{\text{MMP-2}}^{\text{SMC}}(\tau)$ [fg]	$m_{\text{MMP-2}}^{\text{SMC}}(\tau) = M_{\text{MMP-2}}^1 (\exp(-(\tau - \tau_{\text{phys}})/\kappa_{\text{MMP-2}}^1) - 1)$ $\tau_{\text{phys}} = 3 \text{ Pa}$ $M_{\text{MMP-2}}^1 = 2.656 \times 10^{-5} \times T \text{ [fg]}$ $\kappa_{\text{MMP-2}}^1 = 1 \text{ Pa}$ $T \text{ [hours]}$	 <p>Sakamoto et al (2006), Garanich et al (2005)</p>

Table A2 Stress-dependent factors secretion.

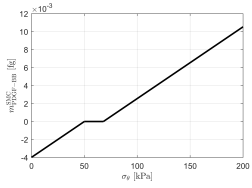
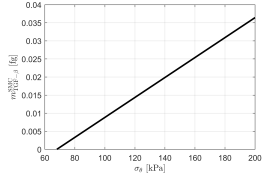
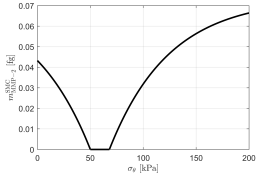
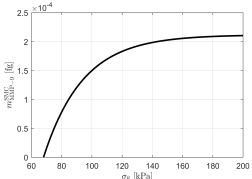
Parameter	Equation	Graphs and References
Mass of PDGF-BB secreted by one SMC (SMC-secreted) $m_{\text{PDGF-BB}}^{\text{SMC}}(\sigma_{\theta})$ [fg]	if $\sigma_{\theta} \geq 68$ kPa: $m_{\text{PDGF-BB}}^{\text{SMC}}(\sigma_{\theta}) = m_{\text{PDGF-BB}} \times \sigma_{\theta} - M_{\text{PDGF-BB}}$ $m_{\text{PDGF-BB}} = 7.98 \times 10^{-5} \times T \text{ [fg}\cdot\text{kPa}^{-1}\text{]},$ $M_{\text{PDGF-BB}} = 5.4264 \times 10^{-3} \times T \text{ [fg]}$ $T \text{ [hours]}$	 <p>Keshavarzian et al (2018), Bayer et al (1999)</p>
Correcting factor for PDGF-BB $C_f(\sigma_{\theta})$ [-]	if PDGF-BB (EC-secreted) > 0 and $\sigma_{\theta} \leq 50$ kPa: $C_f(\sigma_{\theta}) = \beta_{\text{PDGF-BB}}^1 \times \sigma_{\theta} + \beta_{\text{PDGF-BB}}^2$ $\beta_{\text{PDGF-BB}}^1 = 7.98 \times 10^{-5} \times T \text{ [kPa}^{-1}\text{]},$ $\beta_{\text{PDGF-BB}}^2 = -3.99 \times 10^{-3} \times T \text{ [-]}$ $T \text{ [hours]}$	
Mass of TGF- β secreted by one SMC (SMC-secreted) $m_{\text{TGF-}\beta}^{\text{SMC}}(\sigma_{\theta})$ [fg]	if $\sigma_{\theta} \geq 68$ kPa: $m_{\text{TGF-}\beta}^{\text{SMC}}(\sigma_{\theta}) = m_{\text{TGF-}\beta} \times \sigma_{\theta} - M_{\text{TGF-}\beta}$ $m_{\text{TGF-}\beta} = 2.76 \times 10^{-4} \times T \text{ [fg}\cdot\text{kPa}^{-1}\text{]},$ $M_{\text{TGF-}\beta} = 1.8768 \times 10^{-2} \times T \text{ [fg]}$ $T \text{ [hours]}$	 <p>Keshavarzian et al (2018)</p>
$m_{\text{MMP-2}}^{\text{SMC}}(\sigma_{\theta})$ [fg]	$m_{\text{MMP-2}}^{\text{SMC}}(\sigma_{\theta}) = M_{\text{MMP-2}}^2 (1 - \exp(\alpha((\sigma_{\theta} - \sigma_{\theta}^{\text{phys}})/\kappa_{\text{MMP-2}}^2)))$	
Mass of MMP-2 secreted by one SMC	if $\sigma_{\theta} \geq 68$ kPa: $\alpha = -1$ $\sigma_{\theta}^{\text{phys}} = 68 \text{ kPa}$ $M_{\text{MMP-2}}^2 = 7.347 \times 10^{-2} \times T \text{ [fg]},$ $\kappa_{\text{MMP-2}}^2 = 56.28 \text{ kPa}$ $T \text{ [hours]}$	
$m_{\text{MMP-2}}^{\text{SMC}}(\sigma_{\theta})$ [fg]	if $\sigma_{\theta} \leq 50$ kPa: $\alpha = 1$ $\sigma_{\theta}^{\text{phys}} = 50 \text{ kPa}$ $M_{\text{MMP-2}}^2 = 8.67 \times 10^{-2} \times T \text{ [fg]},$ $\kappa_{\text{MMP-2}}^2 = 56.28 \text{ kPa}$ $T \text{ [hours]}$	<p>Keshavarzian et al (2018) Bayer et al (1999)</p>
Mass of MMP-9 secreted by one SMC $m_{\text{MMP-9}}^{\text{SMC}}(\sigma_{\theta})$ [fg]	if $\sigma_{\theta} \geq 68$ kPa: $m_{\text{MMP-9}}^{\text{SMC}}(\sigma_{\theta}) = M_{\text{MMP-9}} (1 - \exp(-((\sigma_{\theta} - \sigma_{\theta}^{\text{phys}})/\kappa_{\text{MMP-9}})))$ $\sigma_{\theta}^{\text{phys}} = 68 \text{ kPa}$ $M_{\text{MMP-9}} = 2.118 \times 10^{-4} \times T \text{ [fg]},$ $\kappa_{\text{MMP-9}} = 26 \text{ kPa}$ $T \text{ [hours]}$	 <p>Keshavarzian et al (2018)</p>

Table A3 SMC dynamics implemented in the ABM.

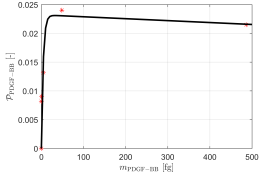
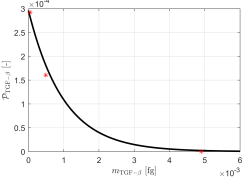
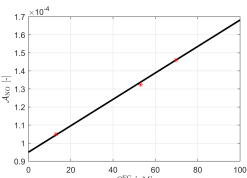
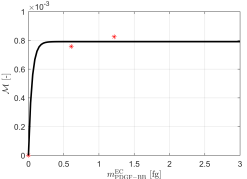
Event	Equation	Graphs and References
SMCs proliferation probability for one SMC in one T \mathcal{P} [-]	$\mathcal{P} = \mathcal{P}_{\text{basal}} + \mathcal{P}_{\text{PDGF-BB}} + \mathcal{P}_{\text{TGF-}\beta}$ $\mathcal{P}_{\text{basal}} = 1.46 \times 10^{-4}$ $\mathcal{P}_{\text{PDGF-BB}} = A_{\text{PDGF-BB}}^1 (1 - \exp(-m_{\text{PDGF-BB}}/\omega_{\text{PDGF-BB}}^1)) + \alpha A_{\text{PDGF-BB}}^2 \times m_{\text{PDGF-BB}}$ $A_{\text{PDGF-BB}}^1 = 2.323 \times 10^{-2}$ $m_{\text{PDGF-BB}} = m_{\text{PDGF-BB}}^{\text{SMC}} + m_{\text{PDGF-BB}}^{\text{EC}} \text{ (from diffusion)}$ $+ C_f \times m_{\text{unit}} [\text{fg}],$ $\omega_{\text{PDGF-BB}}^1 = 4.33 \text{ fg}$ $\alpha = -1$ $A_{\text{PDGF-BB}}^2 = 3.35 \times 10^{-6}$ $m_{\text{unit}} = 1 \text{ fg}$ $\mathcal{P}_{\text{TGF-}\beta} = A_{\text{TGF-}\beta} \exp(-m_{\text{TGF-}\beta}/\omega_{\text{TGF-}\beta}),$ $A_{\text{TGF-}\beta} = 2.936 \times 10^{-4},$ $m_{\text{TGF-}\beta} = m_{\text{TGF-}\beta}^{\text{SMC}} + m_{\text{TGF-}\beta}^{\text{EC}} \text{ (from diffusion)} [\text{fg}]$ $\omega_{\text{TGF-}\beta} = 10^{-3} \text{ fg}$	  <p>Wolf et al (2005), Cucina et al (1998)</p>
SMCs apoptosis probability for one SMC in one T \mathcal{A} [-]	$\mathcal{A} = \mathcal{A}_{\text{basal}} + \mathcal{A}_{\text{NO}}$ $\mathcal{A}_{\text{basal}} = 1.46 \times 10^{-4}$ $\mathcal{A}_{\text{NO}} = \gamma_{\text{NO}} \times (C_{\text{NO}}^{\text{EC}} - {}^{\text{phys}}C_{\text{NO}}^{\text{EC}})$ $\gamma_{\text{NO}} = 7.317 \times 10^{-7} \text{ nM}^{-1}$ ${}^{\text{phys}}C_{\text{NO}}^{\text{EC}} = 69.7 \text{ nM}$	 <p>Krick et al (2002)</p>
SMCs migration probability for one SMC in one T \mathcal{M} [-]	$\mathcal{M} = A_{\text{PDGF-BB}} (1 - \exp(-m_{\text{PDGF-BB}}^{\text{EC}}/\omega_{\text{PDGF-BB}}))$ $A_{\text{PDGF-BB}} = 7.913 \times 10^{-4},$ $m_{\text{PDGF-BB}}^{\text{EC}} \text{ (from diffusion)} [\text{fg}]$ $\omega_{\text{PDGF-BB}} = 4.9 \times 10^{-2} \text{ fg}$	 <p>Dardik et al (2005), Bornfeldt et al (1994)</p>

Table A4 ECM dynamics implemented in the ABM.

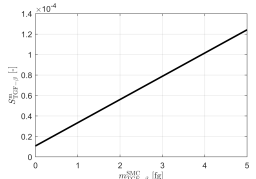
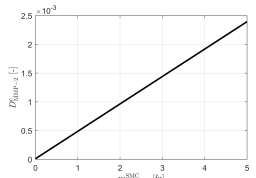
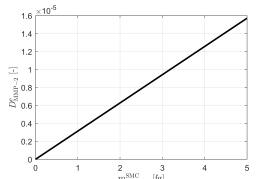
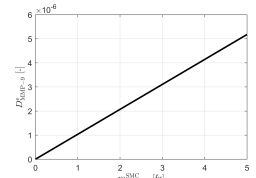
Event	Equation	Graphs and References
Collagen synthesis probability in media for one SMC in one T \mathcal{S}^m [-]	$\mathcal{S}^m = \mathcal{S}_{\text{basal}}^m + \mathcal{S}_{\text{TGF-}\beta}^m$ $\mathcal{S}_{\text{basal}}^m = 1.07 \times 10^{-5}$ $\mathcal{S}_{\text{TGF-}\beta}^m = \gamma_{\text{TGF-}\beta} \times m_{\text{TGF-}\beta}^{\text{SMC}}$ $\gamma_{\text{TGF-}\beta} = 2.27 \times 10^{-5} \text{ fg}^{-1}$ $m_{\text{TGF-}\beta}^{\text{SMC}} [\text{fg}]$	 <p>Keshavarzian et al (2018), Zahedmanesh and Lally (2012)</p>
Collagen synthesis probability in intima for one SMC in one T \mathcal{S}^i [-]	$\mathcal{S}^i = \mathcal{S}_{\text{basal}}^i + \mathcal{S}_{\text{TGF-}\beta}^i$ $\mathcal{S}_{\text{basal}}^i = 2.24 \times 10^{-5}$ $\mathcal{S}_{\text{TGF-}\beta}^i = \mathcal{S}_{\text{TGF-}\beta}^m$	Okada et al (1987)
Collagen degradation probability for one SMC in one T \mathcal{D}^c [-]	$\mathcal{D}^c = \mathcal{D}_{\text{basal}}^c + \mathcal{D}_{\text{MMP-2}}^c$ $\mathcal{D}_{\text{basal}}^c = 1.07 \times 10^{-5}$ $\mathcal{D}_{\text{MMP-2}}^c = \gamma_{\text{MMP-2}}^1 \times m_{\text{MMP-2}}$ $\gamma_{\text{MMP-2}}^1 = 3.5 \times 10^{-4} \text{ fg}^{-1}$ $m_{\text{MMP-2}} = m_{\text{MMP-2}}^{\text{SMC}}(\tau) + m_{\text{MMP-2}}^{\text{SMC}}(\sigma\theta) [\text{fg}]$	 <p>Zahedmanesh and Lally (2012)</p>
Elastin degradation probability for one SMC in one T \mathcal{D}^e [-]	$\mathcal{D}^e = \mathcal{D}_{\text{MMP-2}}^e + \mathcal{D}_{\text{MMP-9}}^e$ $\mathcal{D}_{\text{MMP-2}}^e = \gamma_{\text{MMP-2}}^2 \times m_{\text{MMP-2}}$ $\mathcal{D}_{\text{MMP-9}}^e = \gamma_{\text{MMP-9}} \times m_{\text{MMP-9}}$ $\gamma_{\text{MMP-2}}^2 = 3.1429 \times 10^{-6} \text{ fg}^{-1}$ $\gamma_{\text{MMP-9}} = 1.036 \times 10^{-6} \text{ fg}^{-1}$ $m_{\text{MMP-2}} = m_{\text{MMP-2}}^{\text{SMC}}(\tau) + m_{\text{MMP-2}}^{\text{SMC}}(\sigma\theta) [\text{fg}]$ $m_{\text{MMP-9}} = m_{\text{MMP-9}}^{\text{SMC}}(\sigma\theta) [\text{fg}]$	  <p>Zahedmanesh and Lally (2012)</p>
MMP-2 removal in time T	1% MMP-2	Zahedmanesh and Lally (2012)
MMP-9 removal in time T	MMP-9 / 2.11	Keshavarzian et al (2018)

Table B5 Half-life and diffusion coefficients.

Parameter	Value	References
PDGF-BB diffusion coefficient $\mathbf{D}_{\text{PDGF-BB}}$	$1.26 \times 10^{-7} \text{ cm}^2 \cdot \text{s}^{-1}$	C3ndor et al (2018)
TGF- β diffusion coefficient $\mathbf{D}_{\text{TGF-}\beta}$	$2.13 \times 10^{-7} \text{ cm}^2 \cdot \text{s}^{-1}$	Albro et al (2013)
PDGF-BB half life	2.5 h	Gay and Winkles (1991)
TGF- β half-life	1.6 h	Wakefield et al (1990)